

AGN FEEDBACK AND ENTROPY INJECTION IN GALAXY CLUSTER CORES

ANYA CHAUDHURI¹, SUBHABRATA MAJUMDAR¹, BIMAN B. NATH²

¹Tata Institute of Fundamental Research, 1, Homi Bhabha Road, Mumbai 400005, India and

²Raman Research Institute, Sadashiva Nagar, Bangalore 560080, India

Draft version June 19, 2018

ABSTRACT

The amount and distribution of non-gravitational energy feedback influences the global properties of the intra-cluster medium (ICM) and is of crucial importance in modeling/simulating clusters to be used as cosmological probes. AGNs are, arguably, of primary importance in injecting energy in the cluster cores. We make the first estimate of non-gravitational energy *profiles* in galaxy cluster cores (and beyond) from observational data. Comparing the observed entropy profiles within r_{500} , from the Representative *XMM-Newton* Cluster Structure Survey (REXCESS), to simulated base entropy profiles without feedback from both AMR and SPH non-radiative simulations, we estimate the amount of additional non-gravitational energy, E_{ICM} , contained in the ICM. Adding the radiative losses we estimate the total energy feedback, E_{Feedback} , from the AGN's (the central AGN in most cases) into the clusters. The profiles for the energy deposition, $\Delta E_{\text{ICM}}(x)$, in the inner regions differ for Cool-Core (CC) and Non Cool-Core (NCC) clusters; however the differences in the profiles are much less after accounting for the radiation loss in CC clusters. This shows that although the central AGNs pumps in energy, correlated with the halo mass, the amount of non-gravitational energy remaining in the ICM depends strongly on the amount of cooling in the central region. The total feedback energy scales with the mean spectroscopic temperature as $E_{\text{Feedback}} \propto T_{\text{sp}}^{2.52 \pm 0.08}$, for the entire sample, when compared with SPH simulations derived base entropy profile and $E_{\text{Feedback}} \propto T_{\text{sp}}^{2.17 \pm 0.11}$ when compared with AMR simulations derived base entropy profile. The scatter in the two cases is 15% and 23%, respectively. The mean non-gravitational energy per particle within r_{500} , remaining in the ICM after energy lost in cooling, is $\epsilon_{\text{ICM}} = 2.8 \pm 0.8$ keV for the SPH theoretical relation and $\epsilon_{\text{ICM}} = 1.7 \pm 0.9$ keV for the AMR theoretical relation.

We use the *NRAO/VLA Sky Survey* (NVSS) source catalog to determine the radio luminosity, L_R , at 1.4 GHz of the central source(s) of our sample. For $T_{\text{sp}} > 3$ keV, the E_{Feedback} correlates with L_R , although with different normalization for CC and NCC clusters. Also, CC clusters show a greater radio luminosity for a given value of feedback energy than NCC clusters. For the $T_{\text{sp}} < 3$ keV clusters, E_{Feedback} anti-correlates with L_R . Compared to higher temperature clusters, E_{Feedback} for these lower temperature clusters are also significantly lower (for the similar value of L_R) implying a lower efficiency of feedback. We show that AGNs could provide a significant component of the feedback.

We, further, study the properties of the brightest cluster galaxy (BCG) and estimate the heating provided by them, and find a mild correlation between the BCG heating rate and the feedback energy. Finally, we find that mean mass deposition rate, inside the cooling radius, mildly correlates with the feedback energy.

Subject headings: galaxies: clusters : general – X-rays: galaxies : clusters

1. INTRODUCTION

Galaxy clusters and the intracluster medium (ICM) have long since been a topic of cosmological interest. Their global properties such as gas temperature, X-ray luminosity and SZ-flux, enable one to draw cosmological conclusions from surveys of galaxy clusters (e.g., Reiprich & Böhringer (2002); Vikhlinin et al. (2009); Gladders et al. (2007); Khedekar, Majumdar & Das (2010); Rozo et al. (2010); Sehgal et al. (2011); Benson et al (2013). However, these properties have been useful mostly because they can be predicted from models of structure formation. On the contrary, the detailed properties of the intracluster medium and their evolution with redshift are yet to be satisfactorily understood, since these properties are described by baryonic physics in addition to the dark matter po-

tential in which it resides (e.g. Nath & Roychowdhury (2002); Shaw et al. (2010); Battaglia et al. (2010); Trac, Bode & Ostriker (2011); Chaudhuri & Majumdar (2011)). Several physical processes, such as feedback from galaxies, including active galactic nuclei (AGNs), and/or radiative cooling of the ICM gas, are believed to affect its X-ray properties.

These non-gravitational processes tend to increase the entropy of the ICM, thereby diluting it, and consequently making it under-luminous in X-rays, especially in low temperature (and mass) clusters. Therefore it has been useful to observationally determine the entropy profiles of the ICM and compare with the expectations from various models, with or without feedback. This comparison of the observational entropy with the theoretically predicted values allows one to estimate the degree of feedback. Following the literature, we denote the entropy by $K = k_B T / n_e^{2/3}$, where n_e is the electron number den-

T	The local gas temperature.
T_{sp}	The mean spectroscopic temperature of the cluster.
$K(r)$	The entropy profile as function of radius, $K = k_B T / n_e^{2/3}$ (either observed or theoretical)
K_{obs}	The observed entropy profile.
K_{th}	The theoretical entropy profile from SPH/AMR non-radiative simulations.
M_g	The gas mass enclosed within a radius r .
$K_{\text{obs}}(x)$	The observed entropy profile as function of gas mass .
$x = \frac{M_g(<r)}{M_{500}}$	Gas fraction within radius r (used to denote profiles).
$\Delta K(x)$	Profile for entropy change in a gas mass shell, $K_{\text{obs}} - K_{\text{th}}$.
$\Delta Q(x)$	Non-gravitational energy profile in ICM per unit mass.
$\Delta E_{\text{ICM}}(x)$	The profile for the remnant non-gravitational energy (per particle) in ICM.
$\Delta E_{\text{Feedback}}(x)$	The input energy-feedback (per particle) profile for a cluster.
E_{ICM}	The total non-gravitational energy remaining in the ICM up to a particular radius.
E_{Feedback}	The total energy feedback by central sources given to the ICM up to a particular radius.
$\Delta L_{\text{bol}}(x)$	The energy lost due to cooling in a gas mass shell.
ϵ_{ICM}	Mean non-gravitational energy per particle remaining in the ICM.
$\epsilon_{\text{Feedback}}$	Mean non-gravitational energy per particle which is fed into the ICM by central AGNs.
NCC	Non cool-core
CC	Cool-core
AMR	Adaptive-Mesh Refinement.
SPH	Smoothed Particle Hydrodynamics.

TABLE 1
SYMBOLS AND NOTATIONS USED IN THE TEXT.

sity, T the local gas temperature and k_B , the Boltzmann constant. Note that this entropy is essentially the thermodynamic entropy, which we write as S , shorn of constants and logarithms. Entropy defined in this manner reflects the processes undergone by the gas, such as accretion, gas cooling and feedback. Voit et al. (2005) had shown that in the absence of any feedback and cooling processes, simulations tend to predict a power-law radial profile for the entropy outside the core, with a scaling $K \propto r^{1.1}$, and that their AMR (adaptive-mesh refinement) and SPH (smoothed particle hydrodynamics) simulations agreed to within $\sim 10\%$.

In a previous paper, we have used the observed entropy profiles of the REXCESS survey clusters (see below for details), and expressed the profile as a function not of radial distance, but of gas mass, since entropy per particle is a lagrangian quantity. The physical processes which endow the gas with additional entropy are also likely to move this gas around, and therefore it is better to view the distribution of entropy in gas mass rather than the radial distance (Voit et al. (2005); Nath & Majumdar (2011)). After comparing the observed profiles with the benchmark entropy profile outside the core without feedback, we determine the mean energy deposited per particle in the ICM, and also discovered that the profile of energy deposition has a universal shape (Chaudhuri, Nath & Majumdar (2012); hereafter referred to as CNM12). In this paper, we study the entropy profile in the inner as well as the outer regions.

Voit et al. (2005) found a large discrepancy in the scaled entropy profiles inside the core radii for their AMR and SPH simulations. While SPH simulations form clusters with almost power-law entropy distributions down to small radii, eulerian simulations form much larger cores with the entropy distribution being truncated at significantly higher values. We have used the SPH and AMR simulation results of Voit et al. (2005) both inside and outside the core in order to determine a benchmark en-

trophy profile without feedback, and then compared this with the observed profiles of REXCESS clusters. One of the core motivations of the current work is to provide a platform for better modeling/simulations of Sunyaev-Zel'dovich (SZ) power spectrum and scaling relations including AGN feedback (which has implications for using clusters as cosmological probes). Significant progress has been made in this direction recently, for instance the SPH simulations SZ effect of Battaglia et al. (2010, 2012) using the AGN feedback prescription by Sijacki et al. (2008).

We then discuss our results in light of the emerging scenario of feedback from radio galaxies in clusters. XMM-Newton and Chandra X-ray observations have shown that radio AGN are probably the principal agent heating the hot atmospheres of galaxies, clusters, and groups and suppressing cooling flows, reducing their strength. The main evidence for feedback from radio galaxies comes from the observations of numerous galaxy clusters featuring X-ray deficit low density cavities (Birzan et al. 2008). Our study of the inner region of ICM also becomes important for the implications and connections to the properties of the brightest cluster galaxy (BCG). We adopt a Λ CDM cosmology with $H_0 = 70 \text{ km s}^{-1} \text{ Mpc}^{-1}$, $\Omega_M = 0.3$ and $\Omega_\Lambda = 0.7$.

The plan of the paper is as follows: in §2 we define the cluster sample used in this work, §3 deals with the observed and simulation benchmark entropy profiles, §4 connects the energetics of the cluster to the entropy change in the ICM and §5 deals with AGN feedback. Finally we discuss our findings and conclude in §6 & §7 respectively. In the Appendix, we provide a list of best-fit relations for both SPH & AMR theory profiles.

2. THE CLUSTER SAMPLE

The REXCESS survey (Böhringer et al. 2007) is a subset of the REFLEX cluster catalog, which is a nearly complete flux limited cluster sample, covering 4.24 ster

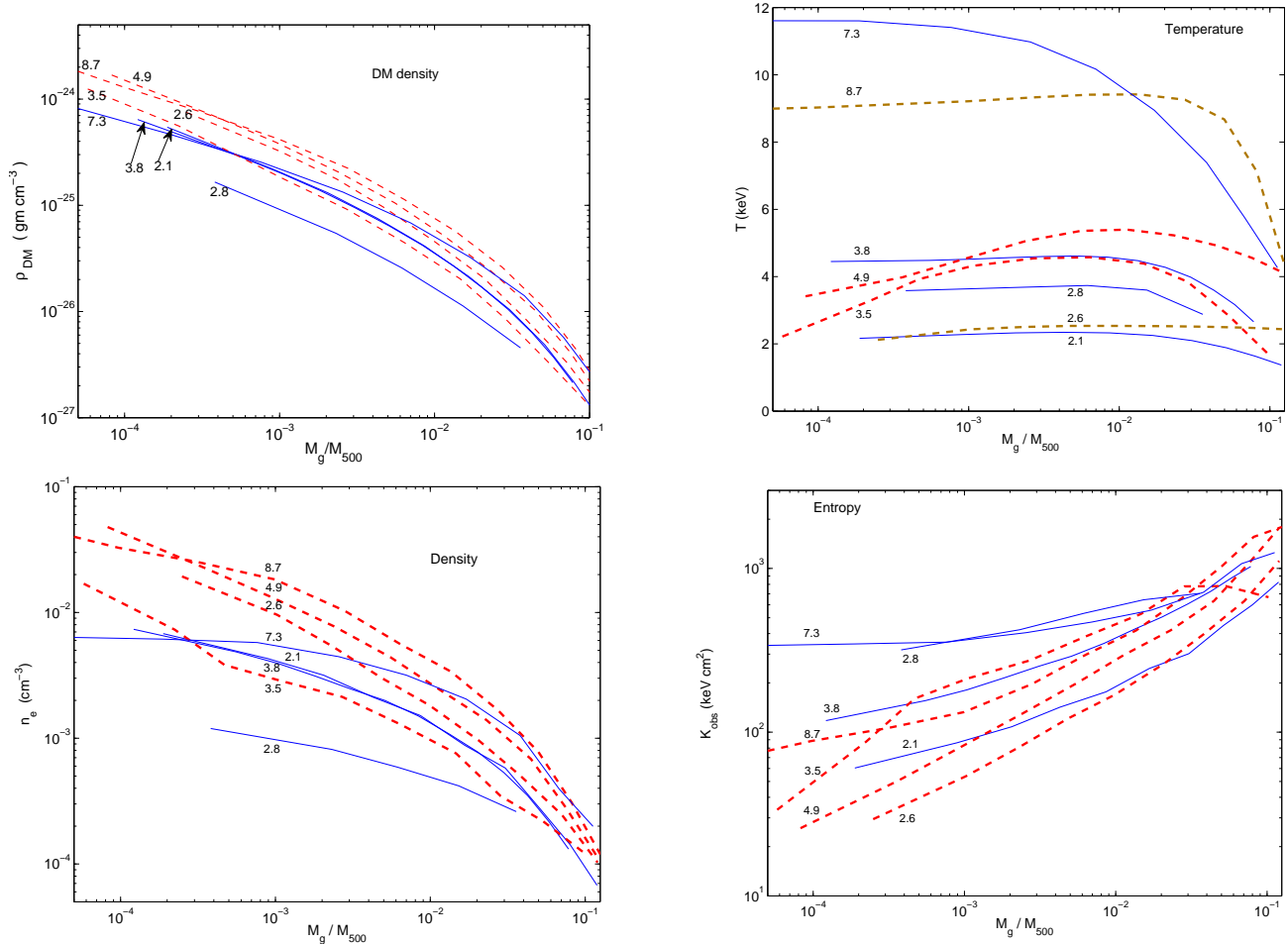


FIG. 1.— Dark matter NFW (Top Left), ICM temperature (Top Right), ICM density (Bottom Left) and ICM entropy (Bottom Right) profiles for a subset of REXCESS clusters. The blue solid lines show NCC clusters while the red dashed lines show CC clusters in all the plots. The clusters are marked by their spectroscopic temperature as given in Table 4 in the Appendix (Also see Table 1 in Pratt et al. (2010)). In the upper right panel, two CC clusters according to REXCESS definition (with $T_{sp} = 8.7$ & 2.6 keV, shown in brown) have temperature profiles that do not fall in the inner regions and have temperature profiles close to NCC clusters.

in the southern extragalactic sky (Böhlinger et al. 2004). The REXCESS sample consists of 31 local clusters ($z \leq 0.2$), where the clusters are selected on the basis of their X-ray luminosity, $L_X = (0.407-20) \times 10^{44} h_{50}^{-2} \text{ erg s}^{-1}$ in the 0.1–2.4 keV band, with no bias for any morphology type. This luminosity range selects clusters with a temperature $\gtrsim 2$ keV, and does not include galaxy groups. Pratt et al. (2010) have noted that the REXCESS sample is well suited to study the variation of entropy profiles across a range of cluster masses, especially because the distances were chosen such that r_{500} fell within the *XMM-Newton* field of view, which increased the precision of measurements at large radii. They also subdivided the sample into CC and NCC systems, defining the clusters with central density $E(z)^{-2} n_{e,0} > 4 \times 10^{-2} \text{ cm}^{-3}$ as CC systems ($E(z)$ being the ratio of the Hubble constant at redshift z to its present value). Some basic properties of the REXCESS clusters are shown in Table 4 (in the Appendix). Our identification of the cluster as CC or NCC (column 6 in the Table) follows the convention used by Pratt et al. (2010).

In Figure 1, we show the Dark Matter (DM) density profiles (top left panel), the ICM temperature profiles (top right panel), the ICM density profiles (bottom left

panel) and the entropy profiles (bottom right panel) for a sub-sample of 4 NCC (shown in blue solid lines) and 4 CC clusters (red dashed lines) selected from the full REXCESS sample. The DM has NFW profiles with a mean concentration parameter 3.2 (for details see §3.2). In the bottom left panel, the ICM density profiles of the CC clusters show a central excess compared to the NCC clusters which leads to the criterion, described above, used by Pratt et al. (2010) in marking CC clusters. In the top right panel, one clearly sees that NCC clusters have flat inner temperature profiles and 2 CC clusters have temperatures going down near the centre indicating cooling. However, 2 CC clusters (in brown dashed lines) are seen to have flat profiles similar to NCC clusters near the centre, showing the simple definition of density excess used to mark CC/NCC clusters may not be robust.

3. ENTROPY PROFILES

3.1. Initial entropy - radial profile

Our goal is to compare the observed entropy profile (as a function of gas mass) with that expected without any non-gravitational processes affecting the ICM. For a baseline entropy profile, with which we will later compare the observed profiles, we turn to the results

of numerical simulations without any radiative cooling. Voit et al. (2005) showed that their simulated SPH profiles can be well described, in the $[0.2-1]r_{200}$ range, by a median scaled profile given by the baseline power law relation, $\frac{K(r)}{K_{200}} = 1.32\left(\frac{r}{r_{200}}\right)^{1.1}$. Their simulated AMR profiles can be similarly well described, in the $(0.2-1)r_{200}$ range, by a median scaled profile given by the baseline power law relation, but with a slightly higher amplitude, $\frac{K(r)}{K_{200}} = 1.41\left(\frac{r}{r_{200}}\right)^{1.1}$.

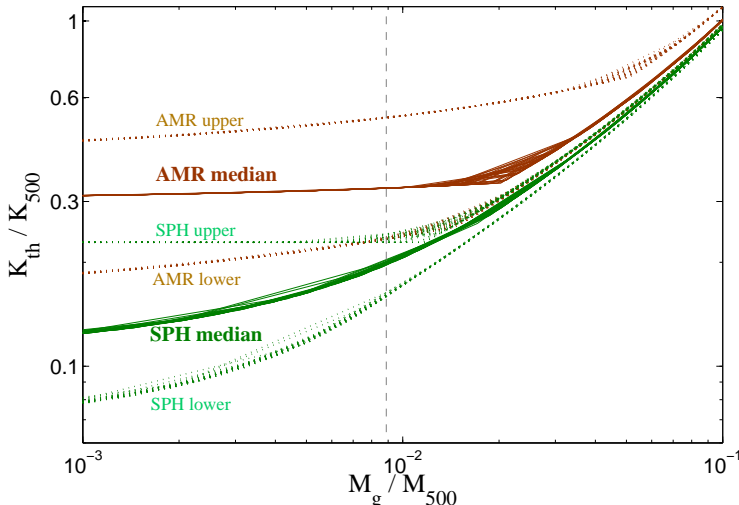


FIG. 2.— The initial scaled entropy profiles, K_{th}/K_{500} , for our sample as a function of gas mass derived from the scaled entropy profiles as function of radii found in non-radiative simulations. The lines correspond to the median relations obtained in the SPH (in green) and AMR (in brown) simulations as well as the envelopes showing the scatter about the median relations (Figure 5 in Voit et al. (2005)). The vertical dashed line corresponds roughly to the average core radii for the cluster sample.

The above SPH relation was used as a benchmark entropy profile in CNM12 for estimating the energy deposition in the ICM outside the core. However, for the ICM inside the core, Voit et al. (2005) found a large discrepancy in the scaled entropy profiles between the SPH and AMR simulations. A flat entropy core has been observed in the centre of non-radiative galaxy clusters in Eulerian grid codes. However this core is absent in Lagrangian approaches such as SPH.

Mitchell et al. (2009) have compared Eulerian simulations to the SPH simulations in the case of an idealized merger between galaxy clusters. They find the discrepancy between the core entropy in the two cases, and of the same magnitude found by Voit et al. (2005) between their AMR and SPH codes. They find that the difference is because of the different treatment of vortices in the two codes. While in the SPH case, the particles retain their initial entropy even after the merger, in the grid case the initial lower entropy is wiped out as a result of the strong vortices generated during the mergers. Vazza et al. (2011) found that the occurrence of a flat entropy core is mainly due to the hydrodynamical processes that are resolved in the Eulerian code, and that additional numerical effects influenced the entropy level to a much lesser degree. We have used the entropy profile ob-

tained as a fit to the SPH simulation data points as well as the AMR simulations obtained by Voit et al. (2005) as our baseline entropy profile. We have fit the SPH median and AMR median profiles, $K(r)$, in the whole radial range with an appropriate fourth order polynomial and used this as the baseline profile to calculate the $K(M_g)$. These two baseline profiles illustrate the uncertainty in the energy calculations due to the assumption of the theoretical profile.

3.2. Initial entropy profile with gas mass

We first calculate the ‘initial’ entropy profile (given above) as a function of gas mass, assuming hydrostatic equilibrium in a Navarro-Frenk-White (NFW) halo (Navarro, Frenk & White 1997) with a concentration parameter $c_{500} = 3.2$. This mean value for the concentration was deduced for a morphologically relaxed cluster sample by Pointecouteau et al. (2005) (see also Pratt et al. (2010)). The condition for hydrostatic equilibrium states that,

$$\frac{dP_g}{dr} = -\rho_g \frac{GM(<r)}{r^2} = -\left[\frac{P_g}{K}\right]^{3/5} m_p \mu_e^{2/5} \mu^{3/5} \frac{GM(<r)}{r^2} \quad (1)$$

where $P_g = n_g k_B T$, is the gas pressure. For the boundary condition, we set the gas fraction inside the virial radius, $f_g(R_{vir})$ to Ω_b/Ω_m . We solve Equation 1 for the pressure profile P_g , from which we determine the ‘initial’ entropy profile $K_{th}(M_g)$, shown in Figure 2, for the case of the AMR median and SPH median profiles as the baseline profile, besides showing the profiles obtained for the envelopes of the AMR and SPH profiles (see Figure 5 in Voit et al. (2005)). The vertical dashed line shows approximately the transition from within-core ($r < 0.1r_{200}$) to outside-core ($0.1r_{200} < r < r_{500}$). Note, that this transition happens over a range in M_g/M_{500} around the vertical line for the cluster sample. In the rest of the paper, we will use the notation $x = \frac{M_g(<r)}{M_{500}}$ to denote ‘profiles’ for any particular entity (for example, $\Delta E(x)$ would refer to energy profile).

4. FRACTIONAL ENTROPY DEVIATION AND ENERGY INPUT

4.1. Non-gravitational energy remaining in the ICM

We follow our previous calculation in CNM12 of energy deposition in this paper to determine the amount of energy deposition associated with the entropy enhancement. We recall that the amount of energy deposition is reflected in the quantity $T\Delta K(x)/K_{obs}$, where $\Delta K(x) = K_{obs} - K_{th}$, since the change in energy per unit mass $dQ = TdS \propto T\Delta K(x)/K$, remembering the distinction between the thermodynamic entropy and the observational definition of entropy.

In CNM12 it was shown that in an isochoric and isobaric processes, (see also (Lloyd-davies et al. 2000)),

$$\begin{aligned} \Delta Q(x) &= \frac{kT}{(\gamma-1)\mu m_p} \frac{\Delta K(x)}{K_{obs}} && \text{(isochoric)} \\ &= \frac{kT}{(1-\frac{1}{\gamma})\mu m_p} \frac{\beta^{2/3}(\beta-1)}{(\beta^{5/3}-1)} \frac{\Delta K(x)}{K_{obs}} && \text{(isobaric)} \end{aligned} \quad (2)$$

The ratio of the changes in energy for a given fractional change $\Delta K(x)/K_{obs}$ and T , for these two cases tends to

γ in the limit of large value of β , and is of order ~ 1.2 for $\beta \leq 2$. For large β , the two estimates of energy input per unit mass can at the most differ by $\gamma \sim 1.67$. Given the simpler expression for the case of isochoric processes, we use the first expression in Equation 2 for our calculation.

We first estimate the energy per particle in the ICM, $\Delta E_{\text{ICM}}(x) = \frac{3}{2} k_B T \frac{\Delta K(x)}{K_{\text{obs}}}$, for each cluster. Figure 3 show the profiles for $\Delta E_{\text{ICM}}(x)/T_{\text{sp}}$, the ratio of the non-gravitational energy in the ICM to $k_B T_{\text{sp}}$ which is indicative of the gravitational potential of the cluster, for the SPH and AMR theoretical relations respectively.

The spectroscopic temperature, T_{sp} , is a good indicator of the gravitational potential of the cluster despite the effects of feedback processes that raise the entropy of the ICM. This follows from the fact that the shocks driven by AGN activity that are likely to deposit energy in the ICM are mostly weak, and observations show that the temperature jump behind the shock is almost non-existent whereas there is a density jump (see, e.g., the discussion by Blanton et al. (2010)). Fabian et al. (2006) suggested the isothermality is caused by efficient thermal conduction, whereas Graham et al. (2008) suggested that mixing of postshock gas with cool gas may erase any sign of temperature rise arising from shocks. Theoretical modeling of the effect of a flux of radio bubbles also show that feedback processes mostly change the density of the ICM in raising its entropy (Roychowdhury et al. 2004, 2005).

In CNM12 we had determined the energy deposition profile outside the core at $M_g/M_{500} \gtrsim 5 \times 10^{-3}$. Our present calculations extend these to inner regions where the effect of feedback is more pronounced. The thick blue (left panels) and red lines (right panels) in Figure 3 show the mean profiles for NCC and CC clusters respectively. The curves show that one can clearly distinguish the cool core clusters from the NCC ones. The profiles for the CC clusters in the inner regions dip significantly with respect to the NCC clusters. This is due to the energy lost by ICM via radiation which is estimated in later sections. Further, the median profiles for the AMR case are lower than those for SPH as the $K_{th}(M_g)$ is much higher for the AMR theoretical relation which is seen in Figure 2.

The theoretical uncertainty in the calculation of $K_{th}(x)/K_{500}$ is illustrated in Figure 4 by showing the mean profile, and the profiles obtained by using the upper and lower envelopes of the benchmark SPH and AMR entropy profiles. The mean profiles of CC and NCC clusters using the median theoretical relation $K_{th}(x)/K_{500}$ are shown in solid red and blue lines respectively, and the profiles corresponding to the lower and upper envelopes of the benchmark profile (shown in Figure 2) are shown with dashed lines respectively. As seen in Figure 2, the three AMR profiles (median and the upper and lower envelopes) and the three SPH profiles differ most inside the core radius which is taken to be $0.1 r_{200}$.

We then integrate the energy deposition profile and determine the total amount of energy injected,

$$E_{\text{ICM}} = \int \frac{kT}{(\gamma - 1)\mu m_p} \frac{\Delta K(x)}{K_{\text{obs}}} dM_g, \quad (3)$$

where the integration is done for mass shells corresponding to region $[0.05-0.5] r_{500}$. Since all clusters have data upto atleast $0.5 r_{500}$, we impose this as the upper radial

cutoff. Similarly, the lower limit $0.05 r_{500}$ is chosen since most cluster profiles have innermost radial points in this region. This lower radial limit corresponds to typical M_g/M_{500} values of 0.0004–0.04. We show the integrated E_{ICM} as a function of cluster temperature in Figure 5 for both the AMR and SPH theoretical relations. The blue stars are for the NCC clusters and the red squares are for the CC clusters. In CNM12 we showed the total energy deposition E_{ICM} vs. cluster temperature, where the calculation was done for profiles outside the core between $0.1 r_{200}$ ($\sim 0.15 r_{500}$) and r_{500} . Here we have looked at the energy deposition between $0.05 r_{500}$ and $0.5 r_{500}$. The ratio of the energy inside the core (i.e., $r < 0.1 r_{200}$) to the total energy within $0.5 r_{500}$ is $\sim 9\%$, and to the energy within r_{500} is $\sim 4\%$. For the SPH case (which was used in CNM12) these are roughly the amounts by which the numbers quoted in CNM12 is underestimated due to the exclusion of the core.

Dividing the total energy by the total number of particles in the ICM, the mean energy per particle, ϵ , can be estimated. Within r_{500} , we find $\epsilon_{\text{ICM}} = 2.81 \pm 0.80$ keV for the SPH theoretical relation, which is comparable to what was found in CNM12. The corresponding value for the AMR theoretical relation is $\epsilon_{\text{ICM}} = 1.69 \pm 0.96$ keV.

4.2. Energy lost due to cooling and feedback energy

In this section we take account of the energy loss due to cooling, which can be calculated from the observed X-ray bolometric luminosity, and estimate the total non-gravitational energy input into the ICM. This can be then connected to the AGN feedback which is done in the next section. In the process of differentiating between the total *energy input* and the non-gravitational *energy retained* in the ICM, we take another look at identifying CC clusters.

We estimate the bolometric luminosity $L_{bol}(x)$ emitted by the ICM using the cooling function Λ_N , approximated by Tozzi and Norman (2001) by a polynomial form for a metallicity $Z = 0.3 Z_{\odot}$. This fit reproduces the cooling function of Sutherland and Dopita (1993) within a few percent in the energy range $kT > 0.03$ keV. In order to estimate the energy lost due to cooling we need to multiply the luminosity by an appropriate time scale, such as the age of the cluster. For this we use the look-back time to the epoch when most of the dark matter potential was in place, since when the cluster mass grew mostly by accretion of gas or minor mergers. Voit et al. (2003) showed that (their Figure 1) for a cluster with present day mass $10^{14} M_{\odot}$, half of its total mass was assembled at a time $t/t_0 \sim 0.6$ ($t_0 = 13.47$ Gyr being the present age of the universe), which corresponds to a lookback time of ~ 5 Gyr (see also Dwarakanath & Nath (2006)). We therefore use $t_{age} = 5$ Gyr for our calculation of energy lost in cooling.

Next, we estimate the *total* energy deposition profile, $\Delta E_{\text{Feedback}}(x)$ by adding the energy lost due to cooling to the energy which has remained in the ICM, i.e.,

$$\Delta E_{\text{Feedback}}(x) = \Delta E_{\text{ICM}}(x) + \Delta L_{bol}(x) \times t_{age}, \quad (4)$$

where $\Delta L_{bol}(x)$ is the energy lost due to cooling in a gas shell and $\Delta E_{\text{Feedback}}$ is calculated for the same radial range as that of ΔE_{ICM} and $x = \frac{M_g(<r)}{M_{500}}$, as before.

Interestingly, although the mean $\Delta E_{\text{ICM}}(x)$ profiles for

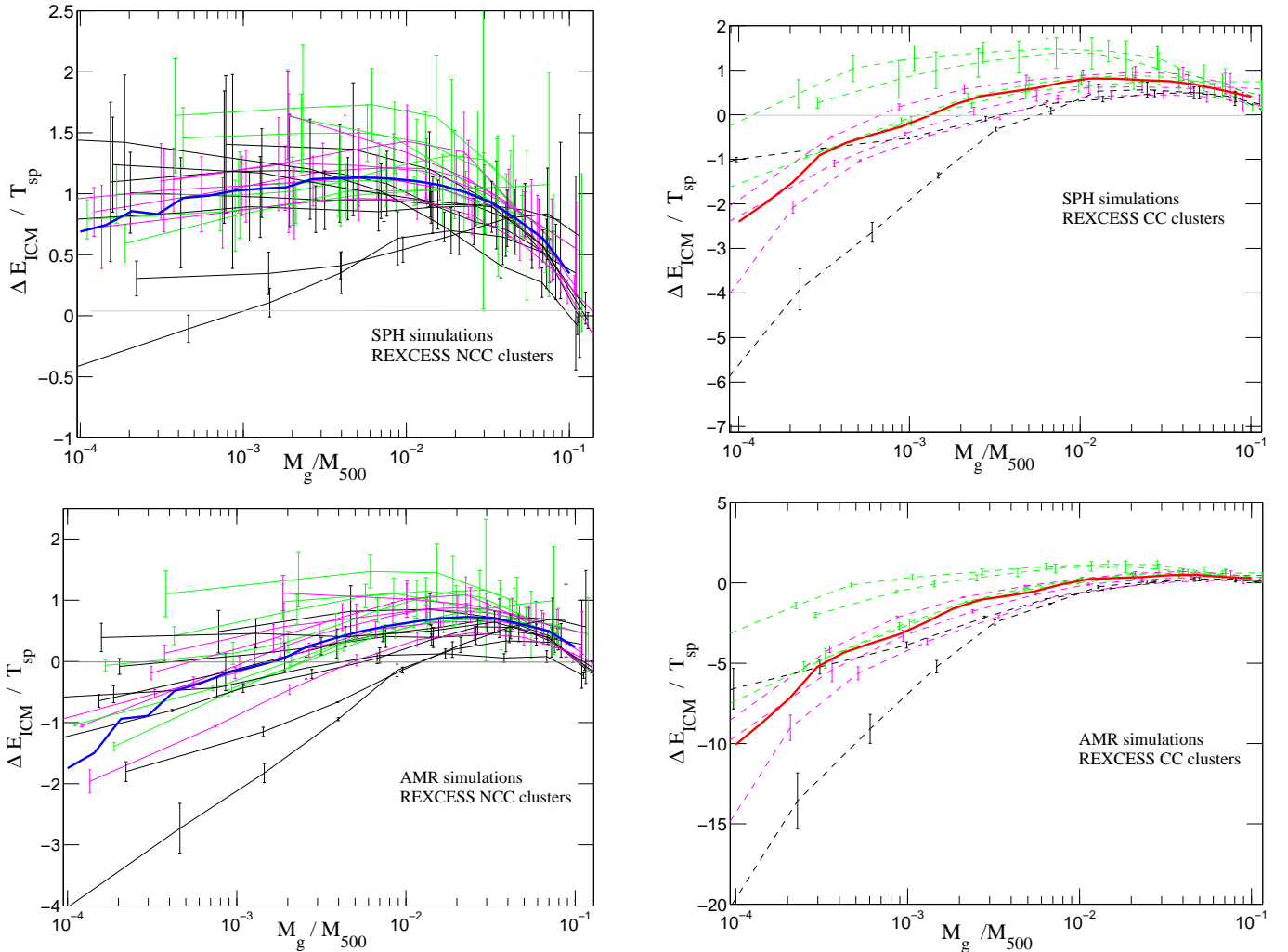


FIG. 3.— The non-gravitational energy in the ICM scaled w.r.t to cluster spectroscopic temperature, $\Delta E_{\text{ICM}}(x)/T_{\text{sp}}$, profiles are shown for the cluster sample for both SPH and AMR benchmark theoretical profiles. The (i) top left panel shows NCC clusters compared to SPH benchmark, (ii) the top right shows CC clusters compared to SPH benchmark, (iii) bottom left shows NCC clusters compared to AMR benchmark, and (iv) the bottom right shows CC clusters compared to AMR benchmark. The *thin* lines show individual profiles for clusters with $T_{\text{sp}} < 3.5$ keV (in green), $3.5 \text{ keV} < T_{\text{sp}} < 5$ keV (in magenta) and $T_{\text{sp}} > 5$ keV (in black). The *thick* blue and red lines show mean profiles for NCC & CC clusters, respectively.

the CC and NCC clusters are different as seen in Figure 3, adding the energy lost due to cooling leads to CC and NCC profiles coming closer at $M_g/M_{500} > 0.001$, especially for the SPH theoretical relation. This is shown in Figure 6.

For the sake of comparison, we plot $\Delta E_{\text{ICM}}(x)$ and $\Delta E_{\text{Feedback}}(x)$ profiles in Figure 7, for the same subsample of clusters as in Figure 1. The thin lines in each panel show the $\Delta E_{\text{ICM}}(x)$ (labelled by the T_{sp} and marked ‘A’), which is the non-gravitational energy remaining in the ICM, and thick lines show the corresponding amount of $\Delta E_{\text{Feedback}}(x)$ (labelled by T_{sp} but marked ‘B’). Thus, one can compare ‘actual’ amount of energy that was put into the ICM given by $\Delta E_{\text{Feedback}}(x)$ which has been partially lost due to cooling leading to the remnant non-gravitational energy in the ICM given by $\Delta E_{\text{ICM}}(x)$. Notice that for NCC clusters, using the SPH benchmark relation, the $\Delta E_{\text{ICM}}(x)$ have positive values at all values of $\frac{M_g}{M_{500}}$ while the CC clusters start to have negative values in the inner regions. In comparison, for the AMR benchmark relation, some NCC clusters have

negative values for $\Delta E_{\text{ICM}}(x)$ in the inner regions; however they become positive quickly when compared to the CC clusters.

Finally, we can calculate the total energy E_{Feedback} by summing over $\Delta E_{\text{Feedback}}(x)$. This E_{Feedback} is shown w.r.t. the spectroscopic temperature T_{sp} in Figure 8. The blue triangles are for the NCC clusters and the red circles are for the CC clusters. The red dot dashed lines, blue dashed lines and the black solid lines show the best fit relations for the CC clusters, the NCC clusters and the combined sample. The relations are also given in the appendix. The corresponding values of the scatter in the $T_{\text{sp}} - E_{\text{Feedback}}$ relation are 21%, 16% and 23% for the AMR theoretical relation and 13%, 15% and 15% for the SPH theoretical relation.

If no energy had been lost in cooling, the ICM *would have got* a higher energy/particle given by $\epsilon_{\text{Feedback}} = 3.46 \pm 0.84$ keV for the SPH theoretical relation and $\epsilon_{\text{Feedback}} = 2.34 \pm 0.78$ keV for the AMR theoretical relation.

In Table 2 we compare the total feedback energy, in

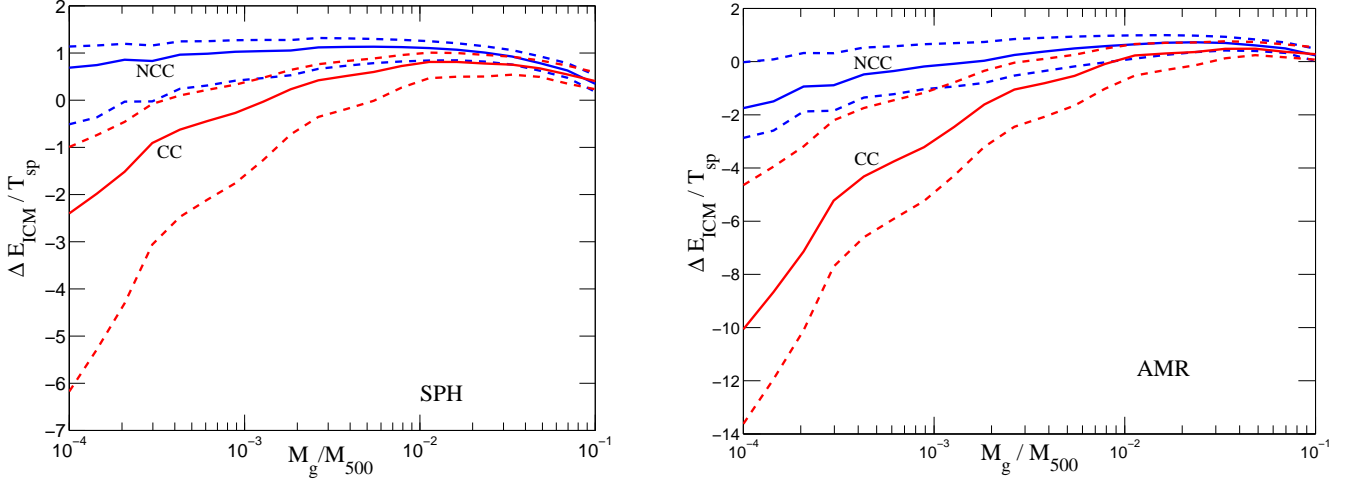


FIG. 4.— The uncertainties in the estimation of $\Delta E_{\text{ICM}}(x)/T_{\text{sp}}$ due to the numerical/theoretical uncertainties in the benchmark profiles are shown. The solid lines are estimated using the median relation in $K_{th}(r)/K_{500}$ in simulations, with red showing CC and blue showing NCC clusters. The red/blue dashed lines show the spread in $\Delta E_{\text{ICM}}(x)$ for CC/NCC clusters due to the spread in the theoretical entropy profiles (Voit et al. 2005). The left panel is for the SPH relations and the right panel is for the AMR relations.

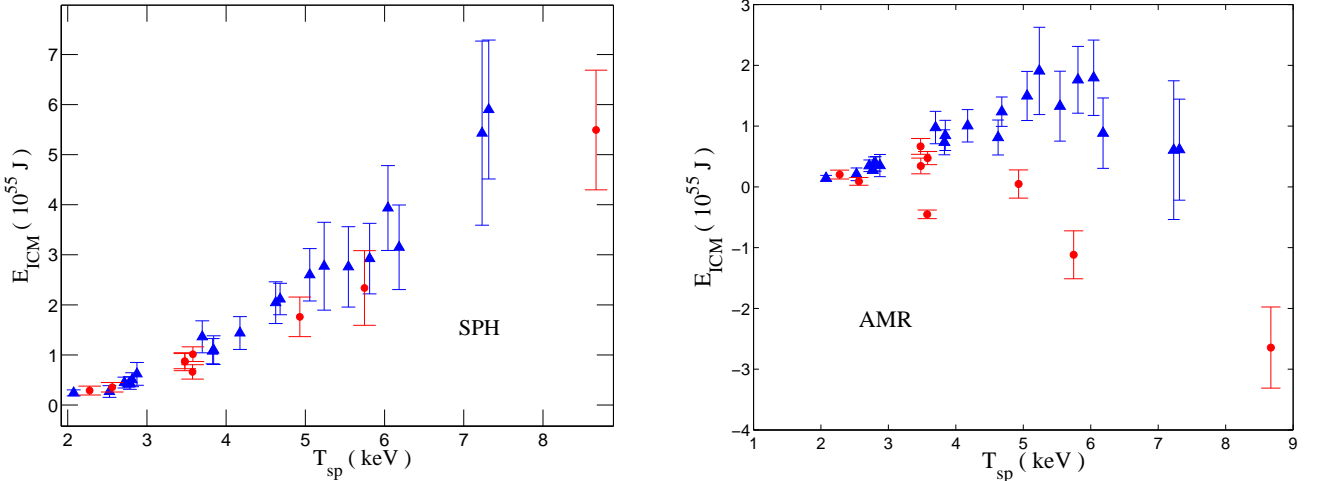


FIG. 5.— The scaling of the *integrated* non-gravitational energy remaining in the ICM, E_{ICM} , (see text for details) with the cluster mean spectroscopic temperature T_{sp} . The solid blue triangles are for the NCC clusters and the solid red circles are for the CC clusters. The left panel is results obtained with the SPH benchmark profile and the right panel for AMR benchmark profile.

the radial range $[0.05-0.5] r_{500}$, when energy lost due to radiative cooling is calculated in two ways: 1) using the luminosity calculated from the theoretical temperature and density profiles, corresponding to the benchmark X-ray entropy profile, and 2) estimated from the observed X-ray luminosities. For the cluster sample, the *observed* E_{Feedback} are smaller than the *theoretical* E_{Feedback} by $\approx 10\%$ for AMR and $\approx 40\%$ for SPH. In our calculations the bolometric luminosity, for all cases, is assumed to be constant for a 5 Gyr period which is taken to be the cluster lifetime. In reality, as the bolometric luminosity would change over the 5 Gyr period from the initial to its final value, the energy lost due to cooling will be bracketed by the observed and theoretical estimated value for each cluster.

Figure 9 shows the relation between E_{Feedback} and the bolometric Luminosity L_X . For a given value of L_X , the E_{Feedback} values are higher for NCC clusters. The blue filled triangles and blue empty triangles are for

the high temperature ($> 3\text{keV}$) and low temperature ($< 3\text{keV}$) NCC clusters. The red-filled and empty circles are for the corresponding CC clusters. The best fit lines are shown by solid lines for the high temperature samples and dashed lines for the high temperature samples. The difference between the CC and NCC clusters is primarily due to the higher luminosity of the CC clusters for the same value of T_{sp} (or equivalently M_{500}). This can be seen in the $E_{\text{Feedback}} - T_{\text{sp}}$ relations for the CC and NCC clusters which are tighter for the two sets of clusters. Roughly, for a given L_X , the ratio $E_{\text{Feedback}}(\text{NCC})/E_{\text{Feedback}}(\text{CC}) \sim 1.7$ for the SPH theoretical relation and ~ 2 for the AMR theoretical relation.

Utilizing the tight relation of E_{Feedback} with T_{sp} , the low temperature and high temperature clusters have been separated by a cut on the y-axis.

5. ENERGY DEPOSITION AND AGN FEEDBACK

We now compare the amount of deposited energy with other observed (or derived) parameters of the clusters

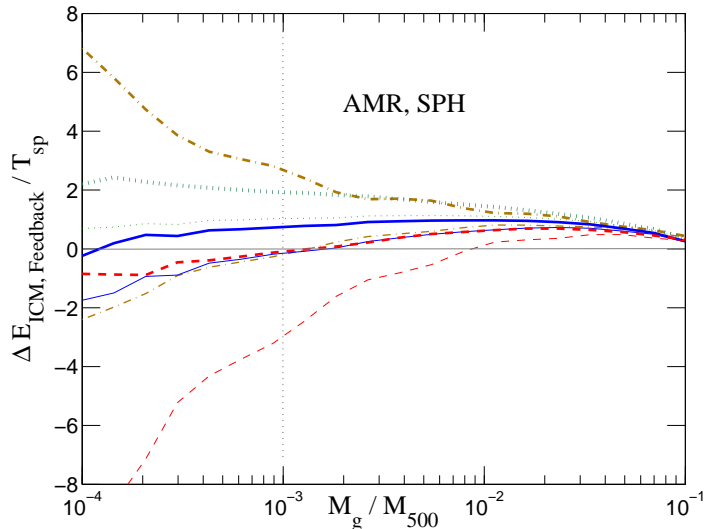


FIG. 6.— Comparison of the mean ΔE profiles for different cases is shown. *Thick lines* are for $\Delta E_{\text{Feedback}}(x)$ with t_{age} taken to be 5 Gyr and corresponding *thin lines* are for $\Delta E_{\text{ICM}}(x)$. The solid blue shows the mean profile for NCC clusters with AMR benchmark relation and the red dashed lines are for the corresponding CC clusters. The brown dot-dashed lines are CC clusters with SPH benchmark relations and green dotted lines are for the corresponding NCC clusters. For visual perception, the horizontal line corresponds to $\Delta E = 0$ and the vertical line approximately marks M_g/M_{500} below which the theoretical benchmark profiles are extrapolated.

that indicate the degree of AGN feedback.

5.1. Central radio luminosity

Although evolutionary effects change the monochromatic radio luminosity of radio lobes for a given jet power to some extent, it is possible to relate radio luminosity at a given frequency to the underlying jet power, which is in turn related to the total feedback energy. The monochromatic radio power remains almost a constant for few tens of Myr. Willott et al. (1999) has found a relation between the jet power and the radio luminosity at 151 MHz, based on the self-similar model of radio galaxy evolution of Kaiser & Alexander (1997). This has been shown to be consistent with the feedback energy in galaxy clusters as determined from X-ray cavities by Cavagnolo et al (2010) (see also Godfrey & Shabala (2013)). Here we use the 1.4 GHz radio luminosity from NVSS as a measure of the underlying jet power of the AGN.

Ma et al. (2011) have found central radio sources in their sample of 400SD clusters between a redshift of 0.1 and 0.6 from the NVSS 1.4 GHz catalog. They have considered all the sources above a flux of 3 mJy, within 250 kpc of the cluster center, where the completeness is 90%. For the background calculation they have used a region between 2° – 4° around the center of the cluster. Considering the uncertainty in the centroids of the clusters and the NVSS resolution, they estimated that the sources within 250 kpc of the center are consistent with being associated with the central galaxy. In this manner they found radio sources within 250 kpc for about 30 % of the clusters. However, they did not find any correlation between the radio power of these sources and the cluster X-ray luminosity, which they found consistent with the fact that their sample is composed of weak and

$E_{\text{AMR}}^{\text{theory}}$	$E_{\text{AMR}}^{\text{obs}}$	$E_{\text{SPH}}^{\text{theory}}$	$E_{\text{SPH}}^{\text{obs}}$
1.18	1.00	1.88	1.34
2.90	2.38	4.54	3.24
2.43	2.33	4.67	3.76
0.70	0.61	1.24	.88
2.93	2.37	4.98	3.53
0.33	0.25	0.58	0.35
0.36	0.27	0.54	00.33
0.37	0.30	0.58	0.38
3.33	3.07	6.58	5.21
1.16	1.26	3.64	2.97
1.62	1.28	2.54	1.71
3.20	3.05	9.85	7.88
0.63	0.49	0.97	0.62
0.27	0.53	1.88	1.64
1.00	0.93	1.94	1.47
0.52	0.41	0.87	0.56
1.02	0.83	1.51	1.04
0.53	2.10	10.79	10.24
2.09	1.82	3.61	2.70
1.54	1.22	2.38	1.61
0.58	1.14	5.17	4.59
0.55	0.44	0.83	0.54
2.69	2.07	4.71	3.17
1.29	1.00	1.90	1.25
0.87	0.77	1.77	1.30
0.57	0.42	0.80	0.49
1.83	1.65	3.80	2.89
2.39	2.22	5.74	4.49
3.29	3.45	10.47	8.74
0.41	0.33	0.92	0.60

TABLE 2
 E_{Feedback} IN 10^{55} J FOR CLUSTERS LISTED IN TABLE 4. THE ENERGY LOST NEEDED TO ESTIMATE E_{Feedback} IS CALCULATED BY USING EITHER 1) X-RAY LUMINOSITY CALCULATED FROM THE THEORETICAL PROFILES, OR 2) OBSERVED X-RAY LUMINOSITY. THE t_{age} HERE IS 5 GYR AND THE RADIAL RANGE FOR CALCULATING E_{Feedback} IS $[0.05 - 0.5] r_{500}$. FOR AMR OR SPH, THE TWO DIFFERENT ESTIMATES OF E_{Feedback} ARE DENOTED BY THE SUPERSCRIPIT "THEORY" AND "OBS", RESPECTIVELY.

non-cooling flow clusters. The average jet power and the AGN heating rate that they have calculated using scaling relations was also not correlated with the X-ray luminosity of the clusters.

For the radio luminosity for the sources in our sample, we have used the NVSS catalogue (Condon et al. 1998). Instead of a fixed physical radius, we have taken a variable radius because the REXCESS clusters are located at a range of redshifts and the value of r_{500} varies significantly. Therefore we have considered radio sources in a region $0.3 r_{500}$ around the central BCG coordinates above a flux of 3mJy. We determined the background contribution as described below. Finally the background subtracted flux of the clusters in the catalog for which such sources exist are listed in Table 3. Clusters 5 ,8, 11, 12, 25, 31 are not in the catalogue as they are south of declination -40° . Cluster 23 with 5 sources in the considered region is excluded. Clusters 4, 7, 17, 24 all of which are NCC clusters do not have a source above 3mJy.

We estimated the background flux by using three annuli far from the cluster center, at $15'-20'$, $20'-25'$ and

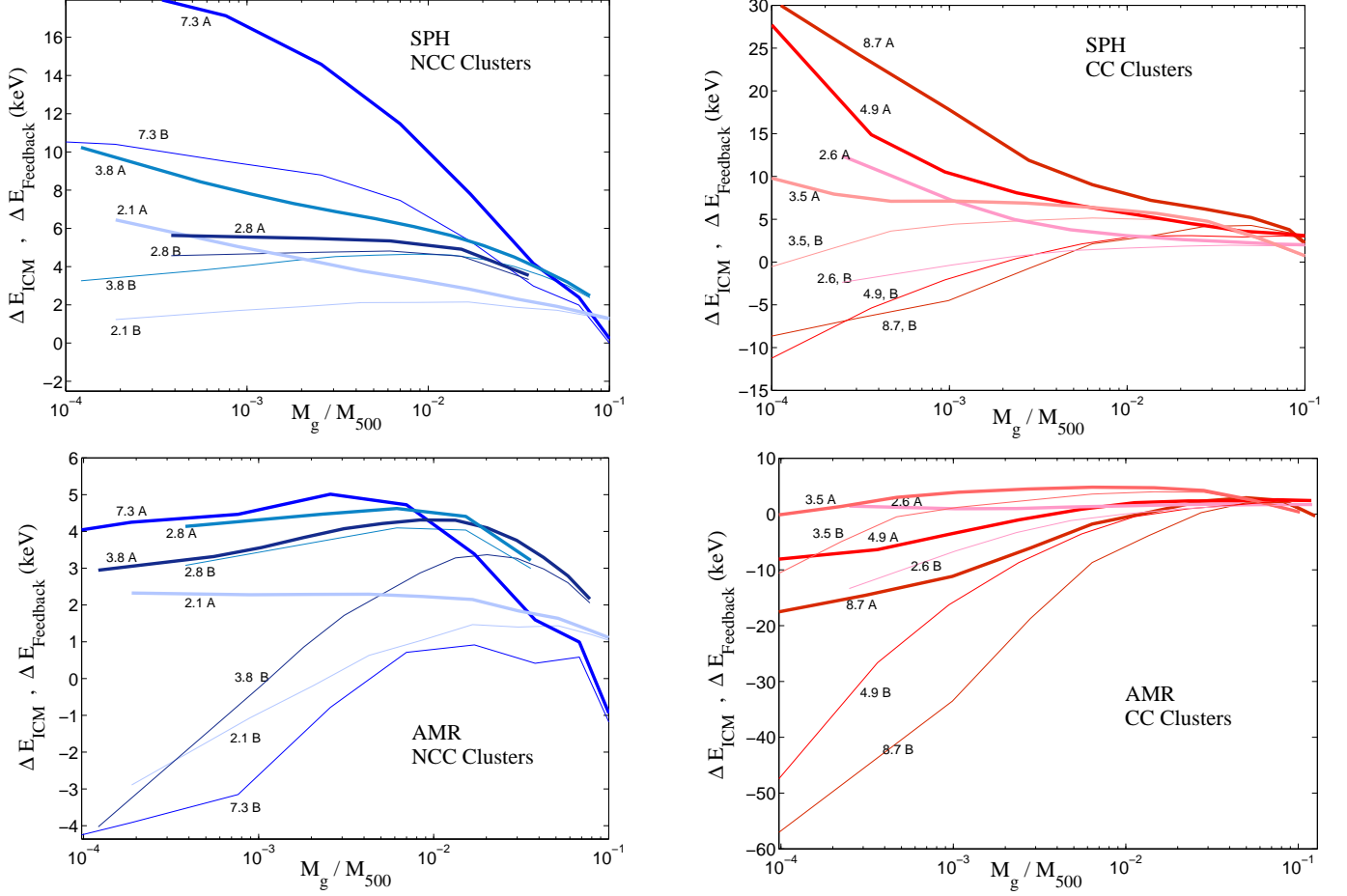


FIG. 7.— The figure shows, simultaneously, the non-gravitational energy remaining in ICM (i.e., $\Delta E_{\text{ICM}}(x)$) and the total non-gravitational energy feedback (i.e., $\Delta E_{\text{Feedback}}(x)$). These are shown for both CC and NCC clusters for the same subset of REXCESS clusters as in Figure 1; each cluster is labeled by their spectroscopic temperature. The left panels are for NCC clusters while the right panels are for CC clusters. Also, upper panels are for SPH and lower panels are for AMR. In each panel, the thick lines marked by the letter ‘A’ show $\Delta E_{\text{Feedback}}(x)$ whereas the thin lines marked by the letter ‘B’ show $\Delta E_{\text{ICM}}(x)$ for the same cluster; the different shades of blue and red are for visual separation of the different clusters.

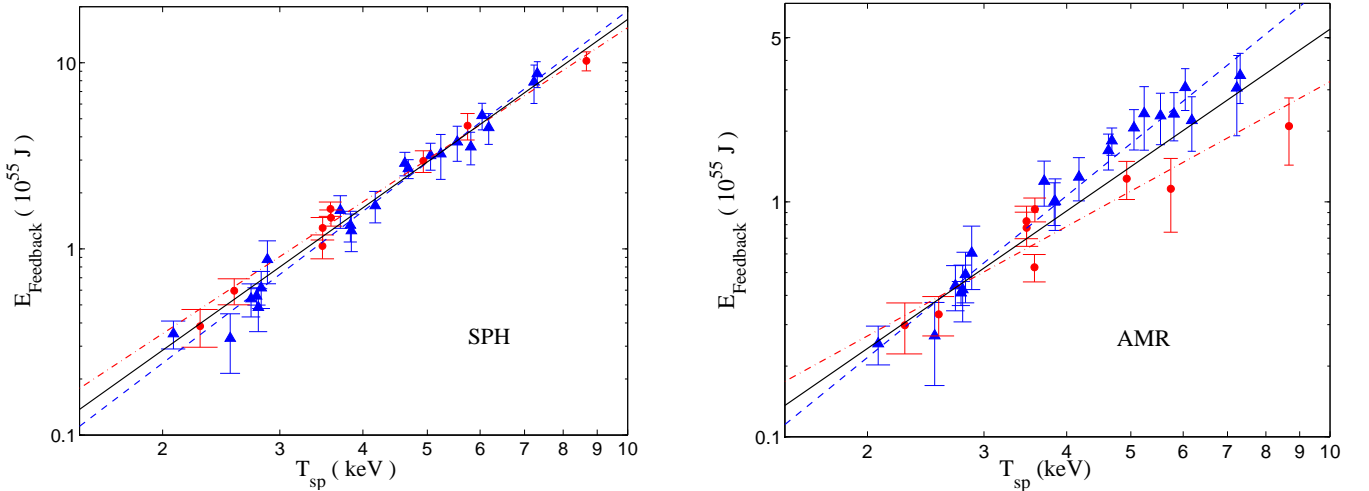


FIG. 8.— The scaling of total energy feedback E_{Feedback} with the cluster mean spectroscopic temperature T_{sp} . The blue triangles are for the NCC clusters and the red circles are for the CC clusters. The best-fit lines for the NCC clusters, the CC clusters and the combined sample are shown by the blue dashed line, the red dot-dashed line and the black solid line respectively. The left panel is for the SPH theoretical relation and the right panel for AMR.

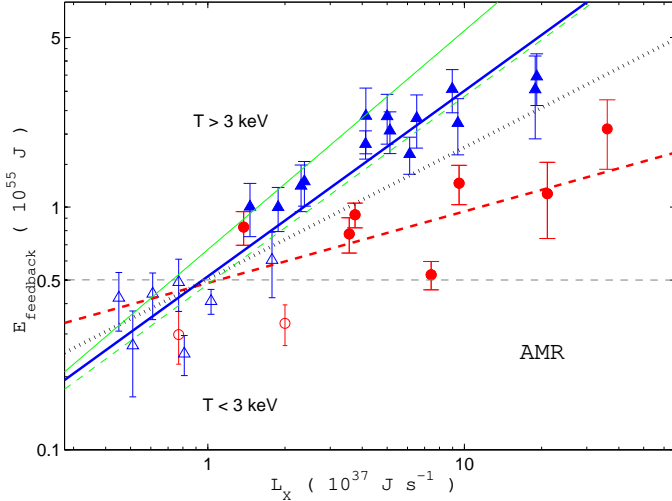


FIG. 9.— The plot shows the correlation between bolometric X-ray luminosity vs the total energy feedback calculated using the AMR benchmark profile. The blue triangles are for NCC clusters, with solid triangles for those clusters with $T > 3\text{keV}$ and the open triangles for clusters with $T < 3\text{keV}$. The solid red circles are for CC clusters with $T > 3\text{keV}$ and the open red circles for CC clusters with $T < 3\text{keV}$. The *thick* solid blue line is the bestfit to the NCC clusters, the *thick* dot-dashed red line is the bestfit to CC clusters and the black dotted is the best fit to the whole sample. For comparison, the *thin* solid and the *thin* dashed green lines shows bestfits for NCC & CC clusters for the SPH benchmark profile.

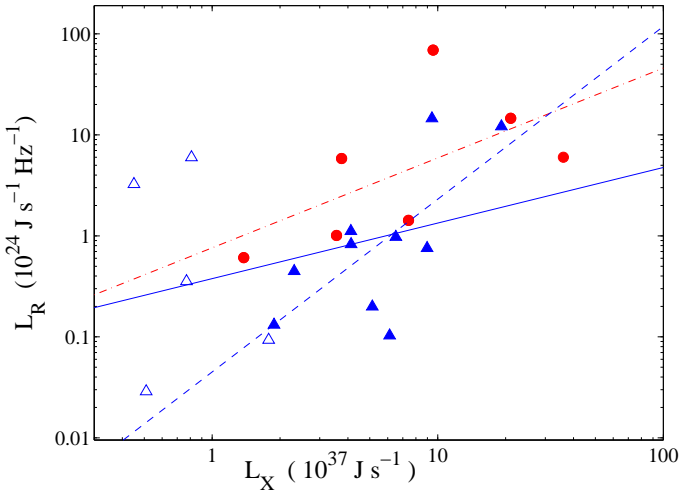


FIG. 10.— This shows the radio luminosity of the central regions of the clusters together with their X-ray luminosity. The blue solid triangles are for the $T > 3\text{keV}$ NCC clusters ; the blue hollow triangles are for the $T < 3\text{keV}$ NCC clusters ; the red solid circles are for the $T > 3\text{keV}$ CC clusters. The blue solid and dashed lines show the bestfits to the total NCC clusters and NCC clusters with $T > 3\text{keV}$ and red dot-dashed line shows the bestfit to the CC clusters.

25'–30'. We calculated the total radio flux in the annuli by summing the radio fluxes of all the sources in them. We then calculated the expected background flux in the region $r < 0.3r_{500}$ by scaling with the ratio of the areas. Table 3 gives the results of the background calculation. The first column is the cluster number as specified in Table 4. The second, third & fourth columns are the total background (in mJy) expected in the region $r < 0.3r_{500}$ derived by scaling the background fluxes found in the annuli 15'–20', 20'–25' and 25'–30', respectively. This is

TABLE 3

THE FIRST COLUMN SHOWS THE CLUSTER NUMBER (CORRESPONDING TO CLUSTER NUMBERS IN TABLE 4); THE SECOND, THIRD AND FOURTH COLUMNS SHOW THE RADIO BACKGROUND IN THE ANNULI OF 15'–20', 20'–25' AND 25'–30'. THE FIFTH COLUMN SHOWS THE AVERAGE VALUE OF THE BACKGROUND. THE FINAL COLUMN SHOWS THE BACKGROUND SUBTRACTED FLUX. NOTE, SOME CLUSTERS ARE MISSING DUE TO REASONS MENTIONED IN THE TEXT.

cluster no.	L_{bin1} (mJy)	L_{bin2} (mJy)	L_{bin3} (mJy)	L_{mean} (mJy)	L_R (mJy)
1	4.23	4.62	10.12	4.45	6.1
2	3.76	3.08	12.48	3.50	24.3
3	6.00	2.17	4.81	4.33	18.4
6	2.02	0.0	0.34	0.20	232.1
9	2.96	13.12	2.13	2.47	12.7
10	5.78	1.44	3.38	2.42	1334.6
13	2.77	3.69	3.48	3.34	21.3
15	0.86	2.46	1.83	1.78	29.8
16	1.03	0.49	4.55	0.80	157.0
18	16.41	2.06	4.04	3.01	34.2
19	5.60	4.92	8.94	6.49	63.4
20	3.83	4.65	5.45	4.64	30.8
21	1.85	1.73	2.16	1.91	12.0
22	2.67	2.23	6.34	2.51	226.7
26	3.14	1.25	11.99	3.77	27.7
27	1.96	8.37	4.10	3.02	406.4
28	2.19	3.14	4.14	2.67	1.7
29	2.58	4.58	4.49	3.79	273.5
30	5.19	1.08	3.17	3.20	196.4

followed by the mean value of the radio background in the three annuli calculated using the two smaller values among the three. The largest value was used only if it is very close to the second largest. This is also because a large value in one of the three cases is always due to a single source with a very high flux. The last column is the background subtracted flux of the radio sources within $r < 0.3r_{500}$ found by using this mean background value.

We find that the background flux estimated from these annuli are similar except in cases where in one of the three annuli, the flux is significantly different because of one source with very high flux. In these case we use only the average of the other two annuli to calculate the background. The similarity of the background flux in at least two of the three annuli shows that the background flux converges at these radii.

A few previous studies have found that there is a relation between the radio luminosity of the central radio source(s) and the X-ray luminosity of CC clusters. Mittal et al. (2009) found that for their 'strong' CC clusters, there is a trend between the bolometric X-ray luminosity and the radio luminosity of the central sources, albeit with considerable scatter. Thus there appears to be a connection between the AGN feedback in the clusters and the global properties such as the X-ray luminosity. They found a correlation coefficient of 0.64 for a power law fit between the two quantities. Ma et al. (2011), however, did not find this correlation for a sample of 400SD clusters with a lack of strong CC clusters. Moreover, they found this lack of correlation between the X-ray luminosity and radio luminosity as well as the X-ray flux and radio flux (Figure 7 and Figure 8 in their paper).

Figure 10 plots the radio luminosity of the central re-

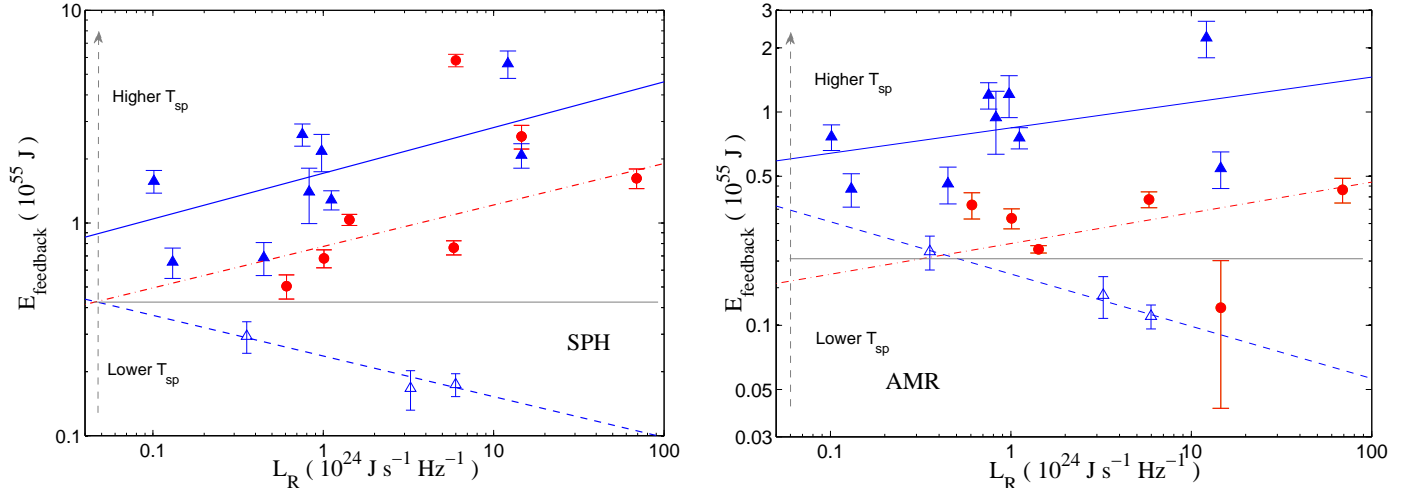


FIG. 11.— Radio luminosity vs the total energy feedback for clusters in the REXCESS sample. E_{Feedback} includes the energy lost in cooling for ~ 5 Gyr. The left panel shows results using the SPH benchmark profile; the right shows for AMR benchmark profile. In both panels, the solid blue triangles are for NCC clusters with $T > 3\text{keV}$, the open blue triangles for NCC clusters with $T < 3\text{keV}$ and the solid red circles are for CC clusters with $T > 3\text{keV}$. The blue solid and the blue dashed lines are the best fits to the NCC clusters with $T > 3$ keV and $T < 3$ keV and the red dot-dashed line is the best fit to the CC clusters. The gradient in the observed mean temperatures of the clusters is indicated by the arrow on the left; the horizontal line roughly divides clusters above and below 3 keV. *Note:* For this figure the data points show E_{Feedback} estimated up to $0.3r_{500}$

gions and the X-ray luminosity of the clusters. The correlation coefficient for a power law relation between L_R and L_X for all the high-temperature ($> 3\text{keV}$) clusters is 0.64. The corresponding values for the high temperature NCC sample are 0.71. The correlation coefficient for the CC sample is 0.71.

Next we plot the amount of deposited energy E_{Feedback} and E_{ICM}^1 against L_R in Figure 11, for the SPH and AMR cases in left and right panels respectively. The panels are divided by horizontal dashed lines to mark the regions of clusters with different ranges of T_{sp} , as determined by the mean relation between E_{Feedback} and T_{sp} obtained earlier. The CC clusters are marked red and NCC clusters are shown in blue. In other words, for a given value of E_{Feedback} , CC clusters are more likely to have a large L_R than NCC clusters. If the central radio luminosity is an indication of feedback processes, this implies that NCC clusters in general have received a large amount of feedback energy, but the central radio luminosity is smaller than in the case of CC clusters.

We perform detailed correlation analysis between E_{Feedback} and L_R for the $T_{\text{sp}} > 3$ keV clusters plotted in Figure 11. For the NCC and CC clusters with AMR benchmark profiles, the correlation coefficients are 0.57 and 0.75, respectively. There are four “non-detected” clusters (No. 4, 7, 17 and 24 listed in Table 4) in the sample of clusters having NVSS plus REXCESS data. All of these are NCC clusters. Of these, only cluster No. 24 has a temperature greater than 3 keV, and is hence considered the lone non-detected cluster relevant for ‘survival analysis’ which is done using the publicly available code ASURV Rev 1.2 (LaValley et al. 1992), which implements the methods presented in Isobe et al. (1986). With survival analysis, the correlation coefficients are 0.52 and 0.75, respectively, for the AMR NCC & CC clusters. This shows that individually they form

¹ Calculated upto $0.3r_{500}$ to make a more meaningful comparison between feedback energy and L_R .

correlated distinct subsamples of the entire cluster population. However, the correlation is lost and becomes 0.06 when NCC & CC are taken together. For completeness, for SPH benchmark profiles, the correlation coefficients for NCC (CC) clusters are 0.60 (0.82) without survival analysis and 0.54 (0.82) with survival analysis.

We also find that the E_{Feedback} for low temperature clusters ($T_{\text{sp}} < 3$ keV) is significantly lower than that of clusters above $T_{\text{sp}} > 3$ keV for the same value of L_R showing a lower efficiency of feedback. We note that the trend between L_R and E_{Feedback} for the low temperature clusters runs opposite to that for high temperature clusters. E_{Feedback} anti-correlates with L_R below this temperature i.e. clusters with a higher value of radio luminosity L_R have a smaller value of E_{Feedback} or a lower efficiency of feedback. However owing to the small sample size of only three clusters in this sample, this result should be taken as tentative.

The monochromatic radio luminosity can be an indicator of the underlying jet luminosity of radio galaxies. Willott et al. (1999) have shown that for FR II radio galaxies, for a period of ≤ 100 Myr, when the jet is active, the radio luminosity does not vary much, and depends mostly on the jet luminosity. They derived a correlation between radio and jet power, based on some model-dependent assumptions, such as self-similar radio lobe evolution and that radio lobes are at minimum energy density. The jet power is however better constrained for FRI radio galaxies from the observations of X-ray cavities. Cavagnolo et al. (2010) found that for FRI galaxies (see their eqn 1),

$$Q_{\text{jet}} \sim 1.1 \times 10^{37} \text{ W} \left(\frac{L_{1.4}}{10^{24} \text{ WHz}^{-1}} \right)^{0.75 \pm 0.14}, \quad (5)$$

where $L_{1.4}$ is the radio luminosity at 1.4 GHz. For FR II galaxies, Godfrey & Shabala (2013) have determined a relation (converting their relation for power at 151 MHz

to 1.4 GHz using a spectral index of 0.6),

$$Q_{jet} \sim g(1.4) \times 10^{37} \text{ W} \left(\frac{L_{1.4}}{10^{24} \text{ W Hz}^{-1}} \right)^{0.67 \pm 0.05}, \quad (6)$$

where the factor g covers many uncertainties. They have concluded that the correlation between radio and jet power for FRI and FRII are broadly consistent, given the large uncertainties. Cavagnolo et al. (2010) estimated a scatter in these relations of order 1.3 dex (see their Fig 2).

The total amount of energy deposited by radio galaxies depends on the total duration for which the jet deposits energy into the ICM. The radio galaxies can have many episodes of activity, each with a life time of order ~ 0.1 Gyr. The duty cycle has been estimated by Best et al (2005) to be $\sim 30\%$. Assuming a time period of ≤ 5 Gyr, which corresponds to the look back time at $z \sim 0.5$ (therefore assuming that radio galaxies formed in these low mass clusters when half of the total mass had been assembled), and a duty cycle of $\sim 30\%$, we get a total energy injected by a radio galaxy of luminosity $10^{23} \text{ W Hz}^{-1}$ to be of order $(1.3\text{--}6.7) \times 10^{54} \text{ J}$ (using eqn 6 and using $g \sim 2$ following Godfrey & Shabala (2013), and using a scatter of 1.3 dex). This is to be compared with the feedback energy in Figure 11, which for this radio luminosity gives a range of $\Delta E_{\text{Feedback}}(x) \sim 3\text{--}10 \times 10^{54} \text{ J}$. The above estimate is in reasonable agreement with this range. Also, for a radio luminosity of $10^{25} \text{ W Hz}^{-1}$, the total feedback energy accumulated for 5 Gyr with a duty cycle of 30% is $\sim (1.5\text{--}30) \times 10^{54} \text{ J}$, comparable to the estimated E_{Feedback} for NCC clusters at this L_R in Figure 11. Therefore the feedback energy in clusters with luminous radio galaxies can be explained by radio galaxies, if they give rise to outbursts with some duty cycle over a period of ~ 5 Gyr. Any shortfall is likely to be filled with other types of AGN different from radio galaxies (Nath & Roychowdhury 2002).

5.2. Correlation between BCG properties and cluster properties

We turn our attention to the properties of the BCG in the cluster and comparisons to cluster properties. Scaling between cluster global properties and BCG properties has been observed in many studies (Brough et al. 2008; Lin & Mohr 2004), for which a variety of reasons have been suggested. Lin & Mohr (2004) have proposed that BCGs could grow in luminosity via mergers with BCGs from subclusters that have fallen into the cluster, and that the BCG would coevolve with the galaxy cluster. It has been shown (Lin & Mohr 2004) that K-band BCG luminosity as determined from the 2MASS K-band magnitudes and the M_{500} of the REXCESS clusters is correlated.

We estimate the heating rate provided by the BCG in the cluster and compare with the E_{Feedback} determined by us and other cluster properties. We use the estimate of Best et al. (2007) for the time averaged heating rate in terms of the stellar mass of the BCG (their Equation 4):

$$\mathcal{H} \sim 2.3 \times 10^{42} (M_*/10^{11} M_\odot) \text{ ergs}^{-1}. \quad (7)$$

Best et al. (2007) derived this by combining the fraction of radio loud galaxies considering the 1.4 GHz luminosity

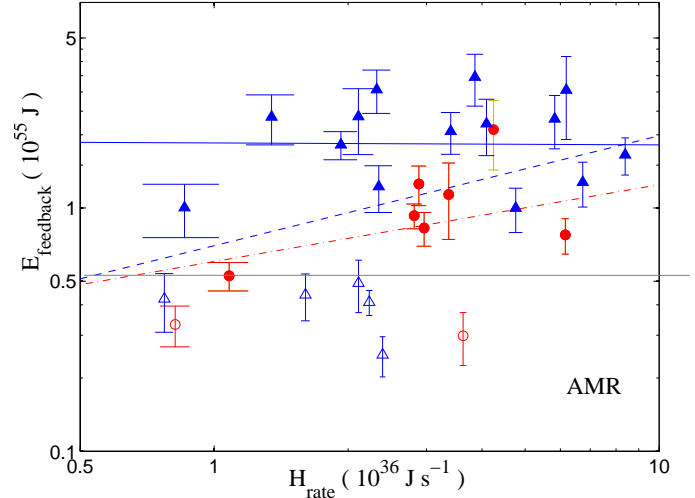


FIG. 12.— The plot shows the correlation between the heating rate, \mathcal{H} , (for details see text) vs the total energy feedback for clusters in the REXCESS sample. The blue triangles are for the NCC clusters, with solid triangles for those clusters with $T > 3\text{keV}$ and the open triangles for clusters with $T < 3\text{keV}$. The solid red circles are for CC clusters with $T > 3\text{keV}$ and the open red circles for CC clusters with $T < 3\text{keV}$. The blue solid and dashed lines show the bestfit to the NCC clusters for the full sample shown the figure and for those with $T > 3\text{keV}$ whereas the red dot-dashed lines is bestfit for $T < 3\text{keV}$ CC clusters in the plot. AMR benchmark profile is used for the calculations. The grey horizontal line shows roughly the $T = 3\text{keV}$ divide.

and the empirical relation found between 1.4 GHz luminosity and the mechanical energy, found in the study of cavities by Birzan et al. (2008). This relation makes no assumption on how the energy is transferred from the AGN to the ICM involved in the above expression since the mechanical energy is directly measured from the cavities and the relation between 1.4 GHz luminosity and mechanical energy is an observed one. The factor f in eqn 3 of Best et al. (2007), that accounts for a range of uncertainties has been set equal to 1 as suggested by Best et al. (2006). We use this expression for the time averaged heating rate of the BCGs in order to compare with E_{Feedback} , the integrated energy deposited over a period of time. We first use the above estimated K-band luminosity of BCGs to determine the stellar mass, using the fits given by Longhetti & Saracco (2009) (their Equation 9b), and finally obtain the heating rate using the above equation. We plot this BCG heating rate with E_{Feedback} in Figure 12.

The correlation coefficient assuming a power law relation between the time-averaged heating rate \mathcal{H} and the Feedback energy E_{Feedback} for the whole sample of clusters are 0.34 and 0.38 respectively for AMR and SPH. The correlation coefficients for the whole CC and NCC samples are 0.05 and 0.28 respectively for AMR and the corresponding values for SPH CC and NCC samples are -0.07 and 0.43. Thus, there is a mild correlation between E_{Feedback} and the time averaged heating rate \mathcal{H} for NCC clusters as well as the combined set. Since \mathcal{H} is the time averaged heating rate due to the brightest cluster galaxies and if the BCG is responsible for a large fraction of the feedback, one would expect the energy deposited by the BCG ($\propto \mathcal{H}$) to be related to E_{Feedback} and hence a correlation.

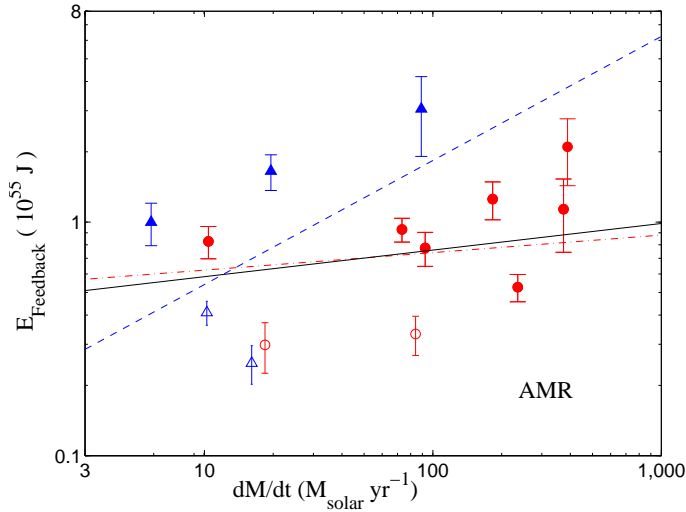


FIG. 13.— The plot shows the correlation between the classical mass deposition rate $\dot{M}_{classical}$ (see text for details) and integrated total energy feedback for clusters in the REXCESS sample. The solid blue triangles are for NCC clusters with $T > 3\text{keV}$ and the open blue triangles for NCC clusters with $T < 3\text{keV}$. The solid red circles are for CC clusters with $T > 3\text{keV}$ and the open red circles for CC clusters with $T < 3\text{keV}$. The best fit lines to the NCC, CC and all clusters in the plot are shown with blue dashed, red dot-dashed and black solid lines.

5.3. Correlation between the mass deposition rate and feedback parameters

The classical mass deposition rate $\dot{M}_{classical}$ can be derived from the density and temperature profiles of each cluster. It is defined as the ratio of the gas mass inside the cooling radius to the cooling time t_{cool} i.e., $\dot{M}_{classical} = M_{gas}(r < r_{cool})/t_{cool}(r_{cool})$. The cooling radius by its usual definition is the radius at which the cooling time is equal to the hubble time, however here r_{cool} is the radius at which $t_{cool} = 5\text{Gyr}$, the age of the cluster used to calculate $E_{Feedback}$. This is a simple measure of the rate at which mass gets deposited and drops out of the X-ray band. This is true, however, if there is no source of heating. Figure 13 shows a plot of energy feedback vs the mass deposition rate. It is evident that NCC clusters has a stronger correlation of The correlation coefficient assuming a power law relation which does not show up for CC clusters². The correlation coefficients assuming a power law relation between $E_{Feedback}$ and $\dot{M}_{classical}$ are 0.6 & 0.57 for the full sample of AMR NCC & CC clusters and 0.6 & 0.87 for SPH NCC & CC clusters. Since, it can be argued that the AGN activity at the centre is influenced by the mass accretion rate, one expects a correlation of $\dot{M}_{classical}$ with the radio power in the cluster centre. Note, that the classical mass deposition rate is not the same as the spectrally determined mass deposition rate, \dot{M}_{spec} which gives the actual observed rate at which gas cools and feeds into the central black hole/s and should be more strongly correlated with the AGN output. Finally, we expect the mass deposition rate to be correlated with the X-ray luminosity in the

² Note, that the bestfit line for the CC clusters is strongly influenced by the extreme left CC cluster which has a high $E_{Feedback}$ and neglecting it would lead to the CC clusters having tighter correlation between $E_{Feedback}$ and $\dot{M}_{classical}$

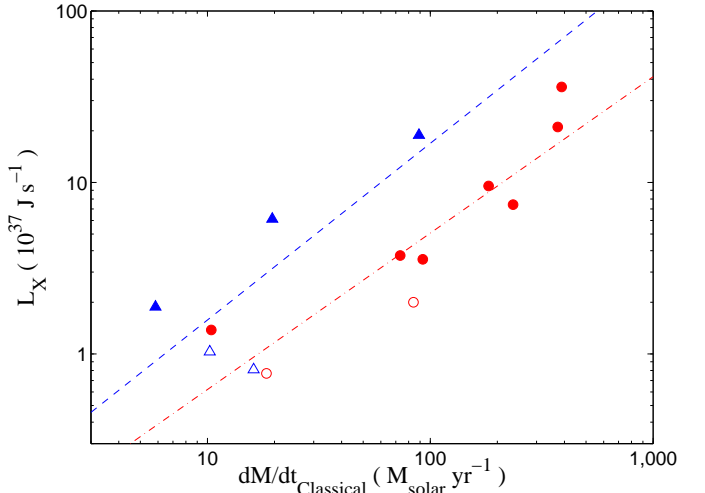


FIG. 14.— The plot shows the correlation between the classical mass deposition rate $\dot{M}_{classical}$ (see text for details) and bolometric X-ray luminosity, within r_{500} , for clusters in the REXCESS sample. The solid blue triangles are for NCC clusters with $T > 3\text{keV}$ and the open blue triangles for NCC clusters with $T < 3\text{keV}$. The solid red circles are for CC clusters with $T > 3\text{keV}$ and the open red circles for CC clusters with $T < 3\text{keV}$. The error bars along both axis are smaller than the marker sizes. The bestfit lines to the NCC and CC clusters in the plot are shown by blue dashed and red dot-dashed lines.

core and this is shown in Figure 14. Notice that for clusters having similar X-ray luminosity, CC clusters show larger mass deposition than NCC clusters, as expected.

6. DISCUSSION

There have been several studies on the dichotomy of CC and non CC clusters exploring the mechanisms that could create and destroy CCs. The two possible processes that have been invoked for the destruction for CCs are major mergers and feedback from a central AGN. Burns et al. (2008) have found that early major mergers prior to $z < 0.5$ are able to destroy nascent cool cores. CC clusters avoid such mergers. In their simulations which had CC and NCC clusters in the same volume, they find that the fraction of CC clusters decreases with mass, as expected due to the relevance of mergers in the formation of higher mass clusters. However they did not find any dependence on redshift. Guo & Oh (2009) have found that the cluster can cycle between the CC and NCC states with the combined effect of a time dependent conduction and AGN outbursts. In this scenario strong AGN heating can bring the CC cluster to the non CC state, which is maintained by conductive heating. Once the conduction is switched off, the cluster is cooled to the CC state with low level AGN heating.

Although it appears that clusters are segregated into mainly two categories, CC and NCC (Cavagnolo et al 2009), there are some clusters which are not easily classified (Rossetti et al. 2011). The latter work found a connection between the presence of giant radio haloes and the absence of CCs. They have explored the 'evolutionary' scenario, where recent and ongoing mergers are responsible for the CC-NCC dichotomy. They have found that all clusters with radio haloes are NCC clusters, showing that processes responsible for the absence of the CC are also associated with the formation of radio haloes, thus lending support to the 'evolutionary' mech-

anism. Combining the number of radio quiet and radio halo clusters with the number of CC and NCC clusters and assuming the lifetime of the radio halo, they find that the relaxation timescale of NCC clusters to CC clusters ranges from 1-2.7 Gyr and that this enables a NCC cluster to relax to the CC cluster.

Rossetti & Molendi (2010) also found regions inside NCC clusters that are characterized by relatively low entropy gas, and concluded that they represent the remnants of a CC after a heating event had converted the rest of the ICM to a NCC state. They found that in most cases of their sample, the heating event was related to merger and in a few cases, with AGN activity.

Our results, in particular the relation between E_{Feedback} and L_R , can be seen to support the above mentioned idea that CC and NCC clusters can be thought of as two different evolutionary stages of clusters in general. We recall that our main findings are: (a) CC and NCC clusters show correlation between injected energy and radio (AGN) luminosity, (b) NCC clusters show a relatively low radio (AGN) luminosity.

To understand these results, we point out two different time-scales that are relevant here: (a) the lifetime of radio galaxies, which is known to be $t_{\text{AGN}} \leq 10^8$ yr e.g. Bird et al. (2008) and (c) the cooling time for NCC clusters to relax to CC state, of order $t_{\text{cool,NCC}} \sim 1-3$ Gyr (see above; Rossetti et al. (2011)). Since the first timescale is much shorter than the time for NCC clusters to turn to CC state, it leads to many NCC clusters without a large value of L_R corresponding to the amount of energy deposition. In most of these cases the ICM in NCC clusters have not yet reverted to the CC state, but the radio source is likely to have faded because $t_{\text{AGN}} \ll t_{\text{cool,NCC}}$. This may explain the fact that NCC clusters in our sample have large E_{Feedback} but not a correspondingly large radio luminosity. In addition, following Rossetti & Molendi (2010), it is also possible that the heating is mediated by merger events, and therefore the NCC clusters do not show large L_R .

7. CONCLUSIONS

By comparing the observed entropy profiles of the REXCESS galaxy clusters to the baseline profile from nonradiative simulations we have determined the total energy change E_{ICM} due to non-gravitational processes in line with CNM12. The profiles $\Delta E_{\text{ICM}}(x)$ for CC and NCC clusters are very different and reach much lower values for CC clusters in the innermost regions due to a greater amount of energy lost due to radiative cool-

ing. Adding to E_{ICM} the energy lost due to cooling we have determined the quantity E_{Feedback} which is the total non-gravitational energy put into the cluster gas, most plausibly, by AGNs in the cluster core. We have studied the scaling relations of the corresponding integrated quantities E_{ICM} and E_{Feedback} with the temperature T_{sp} . The scatter in the $E_{\text{Feedback}}-T_{\text{sp}}$ relation for the SPH and AMR case is 15% and 23% .

We have calculated the radio luminosity L_R of the central radio sources within $0.3r_{500}$ in the REXCESS clusters from the NVSS catalog and find that this quantity is correlated with the bolometric luminosity L_X for both CC and NCC clusters. Typically this behaviour has been observed in CC clusters in other studies. While the high temperature CC and NCC clusters show a positive relation between E_{Feedback} and L_R , the three low temperature NCC clusters in the sample appear to show an opposite trend. For $T_{\text{sp}} > 3$ keV, the $E_{\text{Feedback}}-L_R$ relation shows a strong trend for both the CC and NCC clusters with similar power law slopes for the CC and NCC clusters. The value of L_R in the CC clusters is however much higher than in NCC clusters for the same T_{sp} (or M_{500}) or E_{Feedback} and we observe a separation in the L_R-E_{Feedback} space for the CC and NCC clusters. Energetically, AGN feedback from the central radio galaxies may provide a significant component of E_{Feedback} in both CC and NCC clusters. We have shown that given the uncertainties involved in the estimate of the jet power from radio luminosity, this energy is in reasonable agreement with the required feedback energy that we have calculated.

The utility of large SZ surveys for determining cosmological parameters from cluster abundances and SZ power spectrum is limited by the theoretical uncertainties in their simulations (for example, incorporating energetic feedback from AGNs). Different models of entropy injection and transport would lead to different non-gravitational energy profiles for clusters. In this work, we have made the first estimate of non-gravitational energy profiles in galaxy clusters from X-ray observational data, which can prove useful as benchmark profiles for future simulations to be compared with.

ACKNOWLEDGEMENTS

The authors would like to thank Gabriel Pratt for providing the data on which this work is based, K. S. Dwarakanath for useful discussions and Nissim Kanekar for pointing us out the survival analysis code. SM would like to thank Trevor Ponman for a discussion which led to a closer look at the data and Figure 11.

REFERENCES

- Battaglia, N., Bond, J. R., Pfrommer, C., Sievers, J. L., & Sijacki, D. 2010, ApJ, 725, 91
 Battaglia, N., Bond, J. R., Pfrommer, C., & Sievers, J. L., 2012, ApJ, 758, 74
 Benson, B. A., et al, 2013, ApJ, 763, 147
 Best P. N., Kauffmann G., Heckman T. M., Brinchmann J., Charlot S., Ivezi c Z., White S. D. M., 2005, MNRAS, 362, 25
 Best, P. N., Kaiser, C. R., Heckman, T. M., & Kauffmann, G., 2006, MNRAS, 368, L67
 Best, P. N., von der Linden, A., Kauffmann, G., Heckman, T. M., Kaiser, C. R. 2007, MNRAS, 379, 894.
 Birzan, L., McNamara, B. R., Nulsen, P. E. J., Carilli, C. L., Wise, M. W. 2008, ApJ, 686, 859
 Bird, J., Martini, P., Kaiser, C. 2008, ApJ, 676, 147.
 Blanton, E. L., Clarke, T. E., Sarazin, C. L., Randall, S. W., McNamara, B. R. 2010, PNAS, 107, 7174.
 Böhringer, et al. 2004, A&A, 425, 367
 Böhringer, et al. 2007, A&A, 469, 363
 Brough, S., Couch, W. J., Collins, C. A., Jarrett, T., Burke, D. J., Mann, R. G. 2008, MNRAS, 385L, 103
 Burns, J. O., Hallman, E. J., Gantner, B., Motl, P. M., Norman, M. L. 2008, ApJ, 675, 1125
 Cavagnolo, K. W., McNamara, B. R., Nulsen, P. E. J., et al. 2010, ApJ, 720, 1066
 Chaudhuri, A., & Majumdar, S., 2011, ApJ, 728, L41

- Chaudhuri, A., Nath, B. B., Majumdar, S. 2012, ApJ, 759, 87 [CNM12]
- Condon, J. J., Cotton, W. D., Greisen, E. W., Yin, Q. F., Perley, R. A., Taylor, G. B., Broderick, J. J. 1998, AJ, 115, 1693
- Dwarakanath, K. S., & Nath, B. B. 2006, ApJ, 653, L9
- Fabian, A. C., Sanders, J. S., Taylor, G. B., Allen, S. W. Crawford, C. S., Johnstone, R. M., Iwasawa, K., 2006, MNRAS, 366, 417
- Gladders, M. D., Yee, H. K. C., Majumdar, S., Barrientos, L. F., Hoekstra, H., Hall, P. B., & Infante, L., 2007, ApJ, 655, 128
- Godfrey, L. E. H., & Shabala, S. S. 2013, ApJ, 767, 12
- Graham, J., Fabian, A. C., Sanders, J. S. 2008, MNRAS, 386, 278
- Guo, F., Oh, S. P. 2009, MNRAS, 400, 1992
- Isobe, T., Feigelson, E. D., Nelson, P. I., 1986, ApJ, 306, 490
- Kaiser, C. R., Alexander, P., 1997, MNRAS, 286, 215
- Khedekar, S., Majumdar, S., & Das, S., 2010, Phys. Rev. D, 82, 041301
- LaValley, M., Isobe, T., Feigelson, E. D., 1992, BAAS, 24, 839
- Lin, Y.-T., Mohr, J. J., 2004, ApJ, 617, 879L
- Lloyd-Davies, E. J., Ponman, T. J., & Cannon, D. B. 2000, MNRAS, 315, 689
- Longhetti, M. Saracco, P. 2009, MNRAS, 394, L774
- Ma, C.-J., McNamara, B. R., Nulsen, P. E. J. 2011, ApJ, 740, 51
- Mitchell, N. L., McCarthy, I. G., Bower, R. G., Theuns, T., & Crain, R. A., 2009, MNRAS, 395, 180
- Mittal, R., Hudson, D. S., Reiprich, T. H. & Clarke, T., 2009, A&A, 501, 835
- Nath, B. B., Majumdar, S. 2011, MNRAS, 416, 279
- Nath, B. B., Roychowdhury, S. 2002, MNRAS, 333, 145
- Navarro, J. F., Frenk, C. S., White, S. D. M. 1997, ApJ, 490, 493
- Pointecouteau, E., Aranaud, M., Pratt, G. W. 2005, A&A, 435, 1
- Pratt, G. W., et al. 2010, A&A, 511, A85
- Reiprich, T., & Böhringer, H., 2002, ApJ, 567, 716
- Rossetti, M., Eckert, D., Cavalleri, B. M., Molendi, S., Gastaldello, F., Ghizzardi, S. 2011, A&A, 532, 123
- Roychowdhury, S., Ruszkowski, M., Nath, B. B., Begelman, M. C. 2004, ApJ, 615, 681
- Roychowdhury, S., Ruszkowski, M., Nath, B. B. 2011, ApJ, 634, 90
- Rozo, E., et al., 2010, ApJ, 708, 645
- Sehgal, N., et al., 2011, ApJ, 732, 44
- Shaw, L. D., Nagai, D., Bhattacharya, S., & Lau, E. T., 2010, ApJ, 725, 1452
- Sijacki, D., Pfrommer, C., Springel, V., Enßlin, T. A., 2008, MNRAS, 387, 1403
- Trac, H., Bode, P., & Ostriker, J. P., 2011, ApJ, 727, 94
- Vazza, F., Dolag, K., Ryu, D., Brunetti, G., Gheller, C., Kang, H., & Pfrommer, C., 2011, MNRAS, 418, 960
- Vikhlinin et al., 2009, ApJ, 692, 1060
- Voit, G. M., Balogh, M. L., Bower, R. G., Lacey, C. G., Bryan, G. L. 2003, ApJ, 593, 272
- Voit, G. M., Kay, S. T., Bryan, G. L. 2005, MNRAS, 364, 909
- Willott, C. J., Rawlings, S., Blundell, K. M., & Lacy, M. 1999, MNRAS, 309, 1017

8. APPENDIX

cluster no.	cluster name (RXC)	T_{sp} (keV)	M_{500} ($10^{14} M_{\odot}$)	$M_{g,500}$ ($10^{13} M_{\odot}$)	
1	J0003.8+0203	3.83	2.11	1.99	NCC
2	J0006.0-3443	5.24	3.95	4.48	NCC
3	J0020.7-2542	5.54	3.84	4.06	NCC
4	J0049.4-2931	2.87	1.62	1.66	NCC
5	J0145.0-5300	5.81	4.37	4.85	NCC
6	J0211.4-4017	2.08	1.00	.98	NCC
7	J0225.1-2928	2.53	0.96	.73	NCC
8	J0345.7-4112	2.28	0.97	.82	CC
9	J0547.6-3152	6.04	4.98	5.94	NCC
10	J0605.8-3518	4.93	3.87	4.63	CC
11	J0616.8-4748	4.18	2.70	2.86	NCC
12	J0645.4-5413	7.23	7.38	10.08	NCC
13	J0821.8+0112	2.81	1.31	1.16	NCC
14	J0958.3-1103	5.95	4.17	4.43	CC
15	J1044.5-0704	3.58	2.69	3.32	CC
16	J1141.4-1216	3.58	2.27	2.45	CC
17	J1236.7-3354	2.77	1.33	1.21	NCC
18	J1302.8-0230	3.48	1.89	1.80	CC
19	J1311.4-0120	8.67	8.41	10.69	CC
20	J1516.3+0005	4.68	3.28	3.61	NCC
21	J1516.5-0056	3.70	2.59	2.99	NCC
22	J2014.8-2430	5.75	5.38	7.19	CC
23	J2023.0-2056	2.72	1.21	1.03	NCC
24	J2048.1-1750	5.06	4.31	5.50	NCC
25	J2129.8-5048	3.84	2.26	2.23	NCC
26	J2149.1-3041	3.48	2.25	2.48	CC
27	J2157.4-0747	2.79	1.29	1.12	NCC
28	J2217.7-3543	4.63	3.61	4.37	NCC
29	J2218.6-3853	6.18	4.92	5.67	NCC
30	J2234.5-3744	7.32	7.36	9.87	NCC
31	J2319.6-7313	2.56	1.56	1.74	CC

TABLE 4

BASIC PROPERTIES OF THE REXCESS CLUSTERS. THE FIRST COLUMN IS THE CLUSTER IDENTIFIER NUMBER, THE SECOND COLUMN GIVES THE REXCESS NAME OF THE CLUSTER, THE THIRD COLUMN IS THE SPECTROSCOPIC TEMPERATURE IN THE $0.15 - 0.75 r_{500}$ RANGE, THE FOURTH AND FIFTH COLUMNS SHOW THE TOTAL AND THE GAS MASS WITHIN r_{500} . THE LAST COLUMN MARKS THE CLUSTER AS EITHER NCC OR CC (SEE TABLE 1. IN PRATT ET AL. (2010)).

$\log_{10}(E_{\text{Feedback}}/10^{55} \text{J}) = A + B \log_{10}(T_{\text{sp}}/4\text{keV})$		
SPH	A	B
CC	0.262 ± 0.018	2.32 ± 0.120
NCC	0.214 ± 0.017	2.68 ± 0.111
CC + NCC	0.237 ± 0.013	2.52 ± 0.081
AMR	A	B
CC	-0.068 ± 0.027	1.56 ± 0.229
NCC	0.040 ± 0.020	2.32 ± 0.133
CC + NCC	0.0081 ± 0.016	2.17 ± 0.114

TABLE 5

ABOVE SCALING RELATIONS ARE OBTAINED USING ALL REXCESS CLUSTERS EXCEPT FOR CLUSTER 14 WHICH HAS MUCH LARGER OBSERVATIONAL ERRORS.

$\log_{10}(E_{\text{Feedback}}/10^{55}\text{J}) = A + B \log_{10}(L_X/4 \times 10^{37}\text{Js}^{-1})$		
SPH	A	B
CC	0.148 ± 0.020	0.774 ± 0.042
NCC	0.368 ± 0.018	0.902 ± 0.038
CC + NCC	0.258 ± 0.013	0.768 ± 0.026
AMR	A	B
CC	-0.135 ± 0.025	0.295 ± 0.068
NCC	0.175 ± 0.022	0.765 ± 0.046
CC + NCC	0.030 ± 0.016	0.543 ± 0.037

TABLE 6

ABOVE SCALING RELATIONS ARE OBTAINED USING ALL REXCESS CLUSTERS EXCEPT FOR CLUSTER 14 WHICH HAS MUCH LARGER OBSERVATIONAL ERRORS.

$\log_{10}(E_{\text{Feedback}}/10^{55}\text{J}) = A + B \log_{10}(L_R/5 \times 10^{23}\text{WHz}^{-1})$		
SPH, $0.3 * r_{500}$	A	B
CC	-0.169 ± 0.026	0.195 ± 0.026
NCC > $3keV$	0.169 ± 0.022	0.215 ± 0.0284
NCC < $3keV$	-0.568 ± 0.064	-0.191 ± 0.074
AMR, $0.3 * r_{500}$	A	B
CC	-0.660 ± 0.023	0.144 ± 0.031
NCC > $3keV$	-0.110 ± 0.025	0.119 ± 0.036
NCC < $3keV$	-0.686 ± 0.068	-0.245 ± 0.078

TABLE 7

ABOVE SCALING RELATIONS ARE OBTAINED USING REXCESS CLUSTERS EXCEPT FOR (I) CLUSTER 14 WITH MUCH LARGER OBSERVATIONAL ERRORS, (II) CLUSTERS 5,8,11,12,25,31 WHICH ARE SOUTH OF THE REGION COVERED BY THE NVSS CATALOG, (III) CLUSTER 23 WHICH HAS 5 RADIO SOURCES AND (IV) CLUSTERS 4,7, 17 AND 24 WITH NO SOURCE OVER 3 mJY WITHIN $0.3r_{500}$.

$\log_{10}(E_{\text{Feedback}}/10^{55}\text{J}) = A + B \log_{10}(\mathcal{H}/2 \times 10^{36}\text{Js}^{-1})$		
SPH	A	B
CC	0.172 ± 0.020	0.162 ± 0.073
NCC	0.171 ± 0.020	0.664 ± 0.069
CC > $3keV$	0.243 ± 0.022	0.0128 ± 0.085
NCC > $3keV$	0.471 ± 0.027	0.140 ± 0.078
AMR	A	B
NCC	-0.019 ± 0.023	0.452 ± 0.079
CC > $3keV$	-0.125 ± 0.031	0.316 ± 0.118
NCC > $3keV$	0.265 ± 0.031	-0.008 ± 0.091

TABLE 8

ABOVE SCALING RELATIONS ARE OBTAINED USING REXCESS CLUSTERS EXCEPT FOR (I) CLUSTER 14 WITH COMPARATIVELY LARGER OBSERVATIONAL ERRORS AND (II) CLUSTERS 4 AND 7 WHICH DO NOT HAVE K BAND APPARENT MAGNITUDES IN THE 2MASS CATALOG.

$\log_{10}(E_{\text{Feedback}}/10^{55} \text{ J}) = A + B \log_{10}(\dot{M}_{\text{classical}}/50M_{\odot}\text{yr}^{-1})$		
SPH	A	B
CC	0.066 ± 0.024	0.572 ± 0.041
NCC	0.521 ± 0.062	0.914 ± 0.101
CC + NCC	0.156 ± 0.016	0.450 ± 0.027
CC > 3keV	0.142 ± 0.027	0.286 ± 0.049
NCC > 3keV	0.729 ± 0.066	0.650 ± 0.110
CC + NCC > 3keV	0.282 ± 0.020	0.302 ± 0.033
AMR	A	B
CC	-0.153 ± 0.028	0.0750 ± 0.055
NCC	0.104 ± 0.089	0.531 ± 0.138
CC + NCC	-0.154 ± 0.020	0.114 ± 0.037
CC > 3keV	-0.078 ± 0.031	-0.0513 ± 0.061
NCC > 3keV	0.385 ± 0.095	0.412 ± 0.148
CC + NCC > 3keV	-0.019 ± 0.025	-0.064 ± 0.045

TABLE 9

ABOVE SCALING RELATIONS ARE OBTAINED USING REXCESS CLUSTERS 1, 6, 8, 10, 12, 15, 16, 17, 18, 19, 22, 26, 28 AND 31 WHICH CONSISTS OF CC CLUSTERS AND THOSE NCC CLUSTERS FOR WHICH THE RADIUS r_{cool} CAN BE DEFINED.

$\log_{10}(L_{\text{R}}/5 \times 10^{23} \text{ WHz}^{-1}) = A + B \log_{10}(L_{\text{X}}/4 \times 10^{37} \text{ Js}^{-1})$		
	A	B
CC	0.72	0.89
NCC	0.38	0.24
CC > 3keV	0.73	1.36
NCC > 3keV	0.05	1.69

TABLE 10

ABOVE SCALING RELATIONS ARE OBTAINED USING REXCESS CLUSTERS EXCEPT FOR (I) CLUSTER 14 WITH MUCH LARGER OBSERVATIONAL ERRORS, (II) CLUSTERS 5,8,11,12,25,31 WHICH ARE SOUTH OF THE REGION COVERED BY THE NVSS CATALOG, (III) CLUSTER 23 WHICH HAS 5 RADIO SOURCES AND (IV) CLUSTERS 4,7, 17 AND 24 WITH NO SOURCE OVER 3 mJY WITHIN $0.3r_{500}$.

$\log_{10}(L_{\text{X}}/4 \times 10^{37} \text{ Js}^{-1}) = A + B \log_{10}(\dot{M}_{\text{classical}}/50M_{\odot}\text{yr}^{-1})$		
	A	B
CC	-0.172	0.912
NCC	0.316	1.03
CC + NCC	-0.013	0.721
CC > 3keV	-0.0794	0.700
NCC > 3keV	0.483	0.843
CC + NCC > 3keV	0.133	0.589

TABLE 11

ABOVE SCALING RELATIONS ARE OBTAINED USING REXCESS CLUSTERS 1, 6, 8, 10, 12, 15, 16, 17, 18, 19, 22, 26, 28 AND 31 WHICH CONSISTS OF CC CLUSTERS AND THOSE NCC CLUSTERS FOR WHICH THE RADIUS r_{cool} CAN BE DEFINED.